1-28-2013

Automated Point-of-Care Image Processing Methodology for the Diagnosis of Malaria

Michael B. Jorgensen
University of Connecticut, michael.jorgensen22@gmail.com

Automated Point-of-Care Image Processing Methodology for the Diagnosis of Malaria

Michael Jorgensen

B.S., University of Connecticut, 2011

A Thesis
Submitted in Partial Fulfillment of the
Requirements for the Degree of
Master of Science
at the
University of Connecticut
2013

APPROVAL PAGE

Master of Science Thesis

Automated Point-of-Care Image Processing Methodology for the Diagnosis of Malaria

Presented by

Michael Jorgensen, B.S.

Major Advisor _____

Donald R. Peterson, Ph.D.

Associate Advisor _____

Martin G. Cherniack, M.D.

Associate Advisor _____

Robert A. Levine, M.D.

University of Connecticut

2013

Acknowledgments

First, I would like to sincerely thank my major advisor, Dr. Donald Peterson. Your guidance and leadership have propelled me along this immensely rewarding journey.

To Dr. Robert Levine, thank you for your mentorship, enthusiasm, inspiration, and persistence. Your advice and encouragement were so very important in the conduction of my research and the completion of this thesis. Thank you for all of your help and support throughout this entire process.

To Dr. Martin Cherniack, thank you for your support and helpful contributions. Your input was exceptionally valuable and distinctly strengthened the conclusions of this thesis.

I would like to thank my exceptional colleagues at QDx; Darryn Unfricht, for guiding me in the early stages of my research; Benjamin Ports, for your assistance with consumable and test fixture issues; Cord Mueller, for providing technical support on the imaging system; Niaz Khan, for helping to solve a myriad of programming issues; and Richard Getz, for drafting numerous patent applications and helping to progress this thesis for approval. Thank you to my colleagues at Abbott In Vitro Imaging Systems for their development of the imaging system and their collaboration throughout this project; John Roche, for providing the opportunity for this thesis to transpire; and John Czernikowski for manufacturing the malaria-specific consumables.

Thank you to the Yale Guilford Clinic and Yale New Haven Hospital Hematology Laboratory for generously providing blood specimen. Thank you also to Dr. Choukri Ben Mamoun, and Dr. Peter Krause, for providing malaria cell culture that jumpstarted this research.

Finally, I would like to thank my family and friends. To my parents, Richard and Elizabeth, my sister, Heather, and my brother, Gavin, thank you for always being there and instilling in me that I can do anything I set my mind to. To my girlfriend, Katharine, thank you for your unyielding encouragement and support along the way. To my friends, thank you for your companionship, patience, understanding and support.

Table of Contents

Table of Figures

Table of Tables

Abstract

Malaria has profoundly influenced human history for over four thousand years and despite numerous attempts at eradication, the prevention, diagnosis, and treatment of malaria have been largely ineffective. More than five hundred million people are affected by malaria every year resulting in over one million deaths. Drug resistance development by the parasite has diminished the effectiveness of numerous treatment options due, in part, to overtreatment of negative patients based on insufficient clinical algorithms and diagnostic methods. The goal of this research was to develop an image analysis algorithm to diagnose malaria with a high degree of sensitivity and specificity in addition to performing auxiliary features that offer substantial clinical utility.

The image analysis algorithm was initially implemented using a novel point-of-care hematology analyzer, known as the Abbott Laboratories Imaging Platform (ALIP), for the computation of complete blood counts. This facilitated a simultaneous malaria diagnosis and complete blood count that can be used to confirm or reject malaria infection based on hemoglobin and platelet results. The image analysis algorithm exhibited a sensitivity of 100% and a specificity of 97.7%, outperforming the most commonly used malaria diagnostic instruments. The parasitemia of malaria specimen was automatically calculated to within 0.13% of the actual parasitemia determined by microscopy review. Infected red blood cell indices were calculated and showed a negligible variance in hemoglobin content, but a slight increase in cell volume due to the inclusion of the intraerythrocytic parasite. All four erythrocytic stages were identifiable using the ALIP by the detection of intraerythrocytic hemozoin. All information may be presented to the clinician in less time than any current malaria diagnostic method.

The supplementary information made available by a device like the ALIP allows clinicians to make a more informed diagnosis and determine appropriate treatment methods on a patient-by-patient basis. The application of the image processing methodology with ALIP-like devices will contribute to the early detection of malaria, reduce disease transmission, limit unnecessary exposure to antimalarial drugs, improve resource waste in endemic regions, and has the capacity to save over 100,000 lives annually.

1 Introduction

1.1 The Global Need for Effective Malaria Diagnostics

Malaria is a mosquito-borne parasitic infectious disease caused by the protozoan parasites of the genus *Plasmodium*. There are four species that are infectious to humans, including *falciparum*, *vivax*, *ovale*, and *malariae*, with *falciparum* being the most common and the most fatal.

Malaria affects more than five hundred million people annually resulting in over one million deaths (World Health Organization, 2010), 90% of which occur in children in the sub-Saharan region of Africa. It is the seventh leading cause of death in developing countries and the second leading cause of death due to infectious disease in Africa behind HIV and AIDS. Approximately 3.3 billion people are at risk today, and although antimalarial drugs are commercially available, they are susceptible to resistance development and lack sufficient availability in endemic regions for effective treatment (World Health Organization, 2010). Children can progress to severe malaria within hours and may present with coma, severe anemia, acidosis, and hypoglycemia. Mortality rates have been cited to reach up to 30% even in hospitalized patients (Rafael et al., 2006; World Health Organization, 2006; Greenberg et al., 1989).

A clinical diagnosis based on the patient's symptoms and demographics is the most common and least expensive method of malarial diagnosis (Tangpukdee et al., 2009); however, the symptoms of malaria, which include fever, headache, weakness, chills, dizziness, abdominal pain, nausea, and vomiting, are non-specific and overlap with other common viral or bacterial infections, febrile illnesses, and other tropical diseases. The clinical diagnosis algorithm developed by The Integrated Management of Childhood Illness (IMCI) and introduced by the World Health Organization (WHO) in 1993, exhibits high sensitivity, low specificity, and an over-diagnosis of malaria by 30% (Hawkes et al., 2007).

Overtreatment of negative patients accelerates the evolution of antimalarial drug resistance, complicates the diagnosis of other acute febrile illnesses, and wastes resources in

Figure 1.1: Female *Anopheles* mosquito taking a blood meal. (Centers for Disease Control and Prevention, 2005a)

low-wealth regions that have limited supplies of antimalarial treatment options (Rafael et al., 2006). A prompt and accurate diagnosis is, therefore, imperative to the control and management of malaria.

Delays in diagnosis and treatment are leading causes of malaria-related deaths in several endemic countries, and in non-endemic countries, technicians frequently falsely-diagnose a patient due to lack of experience in examining peripheral blood smears for identification of parasitemia (Tangpukdee et al., 2009). Furthermore, clinicians often doubt microscopy results and continue to treat non-infected patients based on clinical suspicion of the presenting symptoms (Rafael et al., 2006; Reyburn et al., 2004).

1.2 The Malaria Parasitic Life Cycle

The life cycle of the malaria parasite (FIG. 1.2) requires both a vertebrate host and a mosquito for survival. Malaria is spread to humans by an infected female pregnant *Anopheles* mosquito (FIG. 1.1), which releases sporozoites into the vertebrate host during a blood meal.

Sporozoites are highly motile reproductive organisms that travel through the circulatory system and invade the hepatocytes of the liver. An asexual replication process known as schizogony occurs, resulting in the production of tens of thousands (per hepatocyte) of haploid forms, known as merozoites, until the hepatocyte membrane finally ruptures (National Institute of Allergy and Infectious Diseases, 2012).

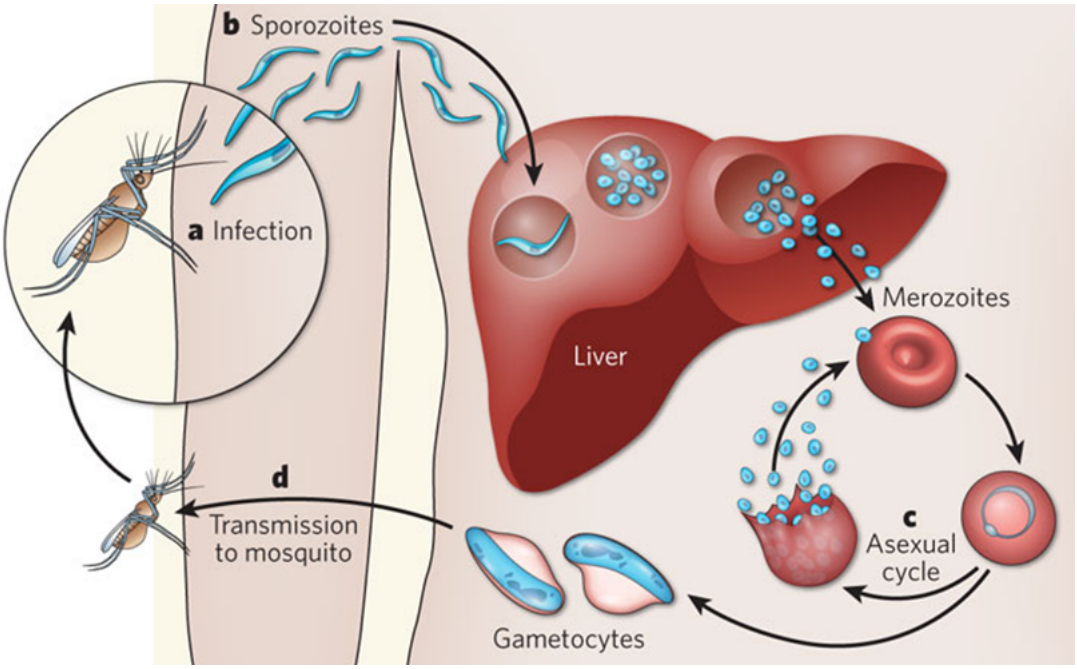

Figure 1.2: Malaria parasite life cycle. (Michalakis et al., 2009)

Merozoites are then released into the blood stream to invade erythrocytes (FIG. 1.3), also known as red blood cells (RBCs), and develop into three morphologically and metabolically distinct stages named rings, trophozoites and schizonts. Merozoites invade RBCs to escape phagocytosis by leukocytes, commonly known as white blood cells (WBCs), and to consume hemoglobin as a protein source for continued replication and survival.

Rings are the first intraerythrocytic stage, evolving over the course of several hours into the larger trophozoite form, which upon initiation of asexual reproduction, begins the schizont stage. Schizonts produce between eight and twenty four daughter merozoites and ultimately rupture the erythrocytic membrane. Each merozoite is then capable of initiating a new cycle of intraerythrocytic asexual replication in a new RBC (Centers for Disease Control and Prevention, 2010c). Schizonts are rarely present in peripheral blood of *P. falciparum* infections, except in severe cases (Centers for Disease Control and Prevention, 2010c). The repeated cycles of development and multiplication within human erythrocytes is responsible for the pathological symptoms associated with human malaria.

During the erythrocytic stage, the malaria parasite consumes hemoglobin and detox-

Figure 1.3: Microscopic image of intraerythrocytic P. falciparum merozoites rupturing an RBC membrane to infect additional RBCs and perpetuate the infection cascade. (National Geographic Society, 2012)

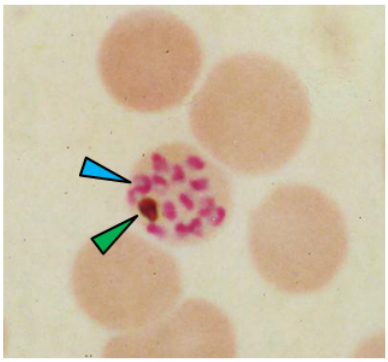

Figure 1.4: Giemsa-stained *Plasmodium falciparum* showing hemozoin (green arrow) in a mature schizont. Blue arrow indicates a single merozoite. (Hempelmann, 2008)

ifies heme by forming an insoluble crystalline brown pigment known as hemozoin (FIG. 1.4). Hemozoin is produced in all erythrocytic stages but is only readily detectable in late trophozoites and schizonts.

A critical step in parasite development, which accounts for the large geographic distribution of malaria worldwide and the rapid spread of drug-resistant strains, is the ability of a subpopulation of the parasites within human red blood cells to differentiate into precursor male and female sexual forms called gametocytes. These forms are transmitted to a female *Anopheles* mosquito during a blood meal. Mating between male and female gametocytes takes place within the mosquito stomach and is followed by meisois and a series of asexual divisions to produce oocysts, each harboring thousands of new sporozoites. In a process known as gliding motility, the sporozoites migrate to the salivary glands of

the mosquito to infect another vertebrate host during another blood meal (Ogunbajo, 2011). This perpetuates the malaria life cycle.

1.3 Babesiosis

Babesiosis is a disease similar in nature to malaria, particularly in terms of its life cycle, cellular morphology, and symptoms that manifest in the human host. Babesiosis is also detectible with the imaging system and therefore it is important to discuss this disease in further detail as well.

The intraerythrocytic protozoa of the genus *Babesia* cause the infectious disease known as Babesiosis. There are over one hundred *Babesia* species that can affect a wide range of hosts, but only a few are documented to infect humans (Vannier et al., 2012). The Northeast is the most endemic region within the United States, where the *B. microti* species is capable of infecting humans primarily between May and October.

The sporozoites of *B. microti* are transferred to a vertebrate host, usually the white-footed mouse (*P. leucopus*), from a tick, primarily *Ixodes scapularis*, during a blood meal (FIG. 1.5) (Vannier et al., 2012). Within the vertebrate host, *Babesia* parasites invade RBCs to avoid leukocyte phagocytosis (FIG. 1.6). Intraerythrocytic replication occurs, producing merozoites that infect more RBCs with a cascade progression similar to malaria. Gametes are differentiated throughout the life cycle and are transferred back to a tick during another blood meal. Gamete fertilization occurs in the gut and the resulting ookinete enters the salivary gland. The ookinete initiates a process known as sporogony that results in the production of sporozoites that are transferred to a human host during a blood meal. The sporozoites do not invade the liver's hepatocytes, as is the case with malaria, but instead directly invade RBCs.

The life cycle of *Babesia* does not perpetuate unless the human host donates blood for transfusion (Vannier et al., 2012). *Babesia* is the most frequently transmitted pathogen by blood transfusion in the United States and, while the occurrence of such an event is rare, this phenomenon is increasing. Furthermore, blood acceptors generally have more a more severe response than tick-transmitted patients, with a mortality rate between

Figure 1.5: *I. scapularis*, commonly known as the deer tick. (Walsh, 2011)

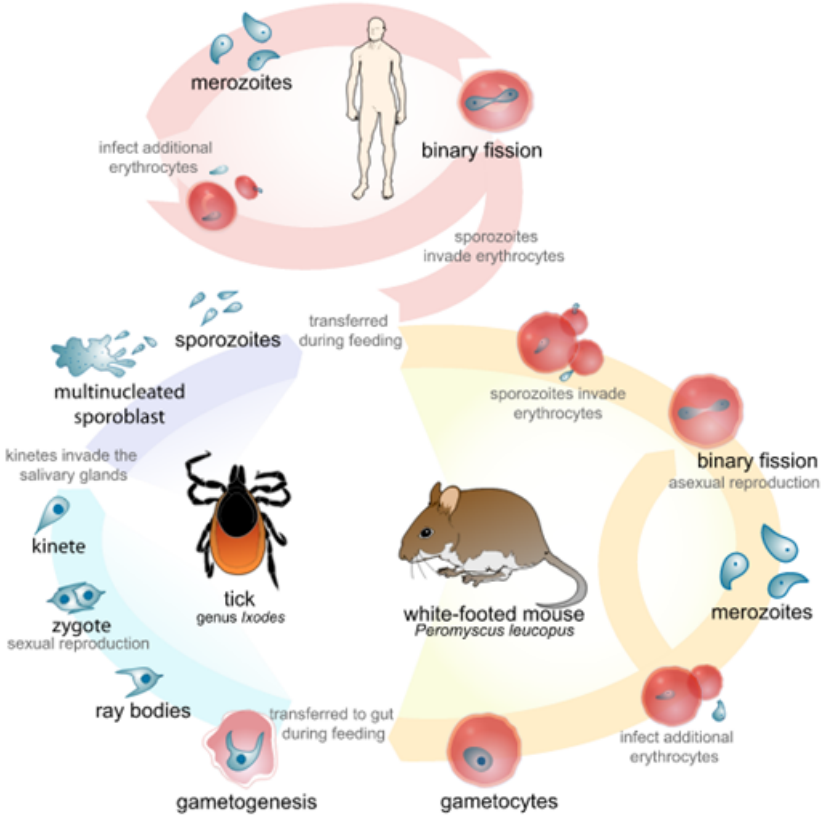

Figure 1.6: Life cycle of the *Babesia* parasite. (Villarreal, 2008; modified and reproduced under the terms of the GNU Free Documentation License)

10% and 28%. Proper screening of blood donors will further decrease the occurrence of transfusion-related infections and mortalities.

Clinical awareness of babesiosis is considerably underestimated because approximately 25% of adults and 50% of children do not present with symptoms (Vannier et al., 2012). Symptoms of babesiosis range from completely asymptomatic to fever, chills, fatigue, nausea, and vomiting. Progression of the disease may be severe or even fatal to asplenic individuals, the elderly, and immunocompromised patients.

1.4 Components of Blood

Considering malaria's inhabitance within the systemic circulation, the components of blood should be discussed in further detail to provide the reader with sufficient background knowledge.

Blood is an essential fluid for oxygen and nutrient transportation to and metabolic waste uptake from the cells of the body. It is comprised of three cell types: RBCs, WBCs, and platelets, all of which are suspended in plasma, a clear to yellow liquid comprised mostly of water, dissolved proteins, and cell nutrients.

1.4.1 Red blood cells

RBCs provide the critical function of delivering oxygen to tissues and circulate throughout the human body for approximately 120 days before being filtered by the kidneys when their supporting proteins are no longer viable (Guyton et al., 2011). RBCs primarily consist of hemoglobin, a metalloprotein responsible for oxygen uptake and distribution throughout the body. Hemoglobin has four identical sub-units, each with a heme component, globin chain, and an iron atom bound to the heme (Guyton et al., 2011). Oxygen has a high affinity to loosely and reversibly bind with iron, thereby enabling RBCs to efficiently transport oxygen molecules.

The cellular structure of the RBC is beneficial to its primary functions (FIG. 1.7). The plasma membrane provides sufficient structure while maintaining compliance, allowing cells to circulate through narrow capillary beds. The biconcave shape optimizes the

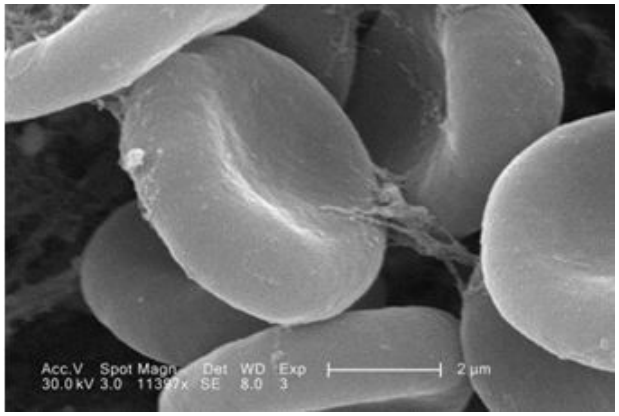

Figure 1.7: Scanning electron micrograph of a red blood cell, magnification 11397X. (Centers for Disease Control and Prevention, 2005b)

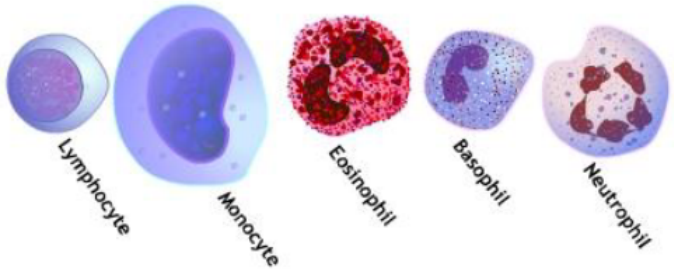

Figure 1.8: The five types of WBCs. In a normal blood sample, the neutrophil is the most common (40-75%), followed by the lymphocyte (20-45%), monocyte (3-11%), eosinophil (0-7%), and basophil (0-1%) (Holmes et al., 2009; RnCeus, 2006).

surface area to improve oxygen transfer across the plasma membrane. RBCs also expel their nucleus during erythropoiesis to allow for maximal hemoglobin content, but immature cells may consist of reticular material for a short period of time while in circulation.

1.4.2 White blood cells

WBCs, shown pictorially in FIG. 1.8, are responsible for the immune response to infection (Guyton et al., 2011). They are subdivided into five subpopulations: neutrophils, lymphocytes, monocytes, eosinophils, and basophils. WBCs are capable of attacking extracellular parasites; however, once a parasite has invaded an RBC, it becomes invisible to most immune responses.

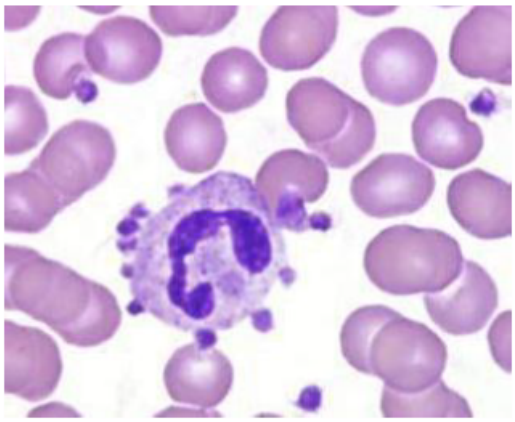

Figure 1.9: Platelets observed with Wright stain, manifesting as small dark-purple fragments. A neutrophil is shown at the center of the image. (Wadsworth Center, 2012)

1.4.3 Platelets

Platelets are cell fragments from megakaryocytes that contribute to hemostasis and blood clotting activity (Guyton et al., 2011). They are shown in FIG. 1.9 in a Wright-stained microscopic image, a common laboratory stain for peripheral blood smear analysis.

1.5 The Complete Blood Count and the Point-of-Care Market

The complete blood count (CBC) is a combination of quantitative and qualitative RBC, WBC, and platelet parameters. It serves as one of the most useful test indicators into a patient's health status and is the most widely ordered blood diagnostics test at over 200 million per year in the United States alone (PixCell Medical, 2010). Diagnoses are not normally decided solely from CBC results but the test can often highlight subtle abnormalities indicating underlying disease development. For decades, the CBC has been reserved for centralized laboratory instrumentation, but the opportunity to perform analyses near the patient presents considerable advantages over current methods.

The imaging system described in this thesis is primarily designed for CBCs in the point-of-care (POC) environment. POC testing is considered any laboratory testing procedure performed outside the centralized laboratory, usually near the patient or even at the bedside. It is one of the most rapidly expanding areas in laboratory medicine (Lewandrowski, 2009) largely due in part to its unique opportunity to increase the oper-

ational efficiency of clinical services (Lewandrowski et al, 2011).

POC hematology analyzers have numerous benefits when compared to centralized testing, including reduced turnaround time, decreased patient length of stay, enhanced efficiency in decision making, improved clinical outcomes, and convenience to clinical staff (Lewandrowski, 2009; Hudson, 2005; Lee-Lewandrowski et al., 2009; Goldsmith, 2004; Lee-Lewandrowski et al., 2010). Many manufacturers are developing POC analyzers to replace the equivalent laboratory test, with new generation devices enabling the test to be permanently performed at the POC (Hudson, 2005). However, a CLIA-waived POC hematology analyzer for CBCs is not currently available due, in part, to limiting federal regulations and the lack of novel technological advances.

It is good clinical practice to perform a CBC on suspect malaria patients because low hemoglobin (anemia) and low platelet count (thrombocytopenia) can be used as confirmatory indicators for disease infection (Giles, 2002; Patel et al. 2004). Anemia, specifically hemolytic anemia, is caused by erythrocyte parasitization resulting in a sudden and dramatic decrease of hemoglobin concentration (HGB) in whole blood (Giles, 2002). Thrombocytopenia is caused by increased splenic sequestration (i.e., blood buildup causing an enlarged spleen), immune-mediated destruction, and a shortened platelet lifespan below the normal two week circulation (Patel et al. 2004). Patel et al. (2004) found that the sensitivity and specificity of diagnosing malaria based exclusively on platelet count (PLT) to be 100% and 70%, respectively (Patel et al. 2004). PLT is therefore an important parameter of the CBC that can be beneficial in diagnosing malaria.

Depending on the duration of infection before the patient presents for laboratory analysis, some flow cytometry analyzers are capable of detecting side scatter of intraerythrocytic or intramonocytic hemozoin; however, they are not sufficiently sensitive, or specific, to be used as a primary method for malaria diagnosis (Wever et al. 2002). The imaging system is inherently capable of performing a CBC and sequentially diagnosing malaria, a feature not available with any hematology technology.

1.6 Prevention of Malaria

The use of insecticides, insecticide-treated bed nets, and drug therapies has and will continue to decrease the prevalence and mortality rate associated with malaria (Jones et al., 2012; Michalakis et al., 2009). However, many populations throughout the world remain at a significant risk of infection because the mosquito resistance to insecticides and artemisinin may contribute to a surge of as many as 26 million new annual cases (Maxmen, 2012a; Maxmen, 2012b). There is no malaria vaccine currently approved for human use but advancements in medical research and technology may offer capabilities to finally eradicate this disease in the future (Jones et al., 2012). Accurate diagnostics also contribute to the prevention of malaria because, the sooner a patient can be diagnosed with malaria, the sooner that patient can be treated with antimalarials to eradicate the parasite, preventing subsequent disease transmission.

1.7 Treatment Methods

Malaria treatment depends on several factors, including disease severity, the *Plasmodium* species, the clinical status of the patient, pregnancy, and the geographic region in which the infection was acquired (Centers for Disease Control and Prevention, 2010b). Intravenous and oral drugs, such as chloroquine, quinine, quinidine, doxycycline, and Artemisinin Combination Therapies (ACT), are generally successful at eradicating uncomplicated cases but certain species of malaria exhibit drug resistance that render some treatments ineffective. ACTs, for example, have demonstrated a 95% cure rate in non-resistant uncomplicated *falciparum* malaria cases (World Health Organization, 2009); however, recent resistance development to artemisinin is concerning and may have severe repercussions. Artemisinin was previously capable of clearing malaria parasites from a patient within 24 hours, but now requires three to four days for a complete treatment (Williams, 2013). In the near future, some patients may not respond to artemisinin at all. Complicating matters further is the prevalence of counterfeit anti-malaria drugs, which contributes to inadequate treatment for the patient and increases the risk of drug resistance development (Bill and Melinda Gates Foundation, 2011).

Treatment based solely on symptoms and without proper diagnosis contributes to resource waste, drug resistance development, and the unnecessary exposure of patients without clinical malaria to antimicrobial agents (Wilson, 2012; Rafael et al., 2006). Further complicating matters is the fact that many people carry and transmit the disease but are asymptomatic of malaria and are not treated (Michalakis et al. 2009). Furthermore, due to the increased cost of newer and more effective drugs, such as artemisinin, diagnostic methods have become vitally important to efficient distribution in resource poor regions (Rafael et al., 2006). The interested reader should refer to the Guidelines for Treatment of Malaria in the United States published by the Centers for Disease Control and Prevention for additional information on prevention and treatment methods (Centers for Disease Control and Prevention, 2011a).

An accurate laboratory diagnosis and knowledge of disease severity, stage progression, and *Plasmodium* species is imperative in formulating a treatment protocol (Centers for Disease Control and Prevention, 2011b). A screening method such as the one proposed in this thesis would permit early diagnosis and treatment of malaria, potentially before the onset of symptoms and disease transmission to another individual. This will help contribute to vector control and by extension, prevent malaria infection.

1.8 Existing Diagnostic Methods and Instrumentation

There are numerous methods available today for the diagnosis of malaria. Each method has its own unique set of advantages and disadvantages, but, to date, an optimal method does not exist. Socioeconomic factors, durability and stability, and distribution limitations are just some of the challenges facing malaria diagnosis.

Two of the most important parameters for a malaria diagnostic test are sensitivity and specificity, both of which are statistical measures of the performance of a binary classification test (i.e., whether or not the patient is infected with malaria). Sensitivity is the proportion of correctly identified positives and is given by

$$Sensitivity = \frac{TP}{TP + FN}\,, \tag{1}$$

while specificity is the proportion of correctly identified negatives and is given by

$$Specificity = \frac{TN}{TN + FP}\,, \tag{2}$$

where TP is the occurrence of true positives, TN is the occurrence of true negatives, FP is the occurrence of false positives, and FN is the occurrence of false negatives.

Two measures closely related to sensitivity and specificity are positive predictive value (PPV) and negative predictive value (NPV). The PPV is the proportion of positive test results that are correct and is given by

$$PPV = \frac{TP}{TP + FP}\,. \tag{3}$$

Conversely, NPV is the proportion of negative test results that are correct and is given by

$$NPV = \frac{TN}{TN + FN}\,. \tag{4}$$

The PPV and NPV of a particular test can provide a clinician with a level of confidence in regards to the accuracy of a given result.

Other features such as parasite morphology assessment, species differentiation, and parasitemia estimation are available in certain methods depending on the diagnostic technology of the test or system. Current diagnostic methods were analyzed in a comprehensive literature review to determine the shortcomings of existent technology and help formulate new ideas to address these issues. A summary of significant findings is described in the following sections.

1.8.1 The Gold Standard Malaria Diagnostic Test: Giemsa-Stained Peripheral Blood Smears and Microscopy Review

The current gold standard for detection of *Plasmodium* employs Giemsa staining of thin and thick blood smears with conventional light microscopy (Tek et al., 2009) (FIG. 1.10). Giemsa is specific to the phosphate groups of DNA and attaches to regions of high

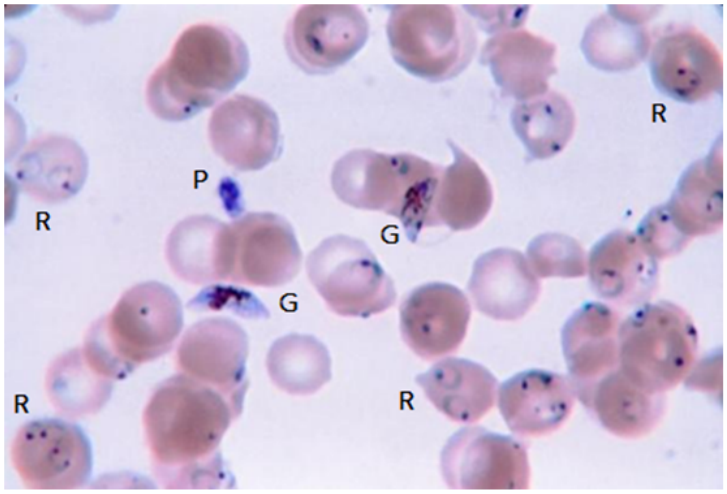

Figure 1.10: *Plasmodium falciparum* Giemsa-stained thin film peripheral blood smear. R indicates ring stage intracellular parasite, G indicates gametocyte, and P indicates platelet. (ScienceDaily, 2007)

adenine-thymine bonding, yielding a high-contrast parasitic visualization. Microscopy review of Giemsa stains is the most commonly-performed laboratory diagnostic test due to its simplicity, relatively low cost, ability to differentiate parasitemia, and manual determination of parasitemia magnitude (Tangpukdee et al., 2009).

Microscopic review of peripheral blood smears suffers from inherent flaws that severely inhibit efficacy in diagnosing malaria. Most importantly, the sensitivity of microscopy is typically no greater than 75% to 90%, and in some settings can be as low as 50% (Wilson, 2012; Rafael et al., 2006). Low parasitemia levels further complicate Giemsa staining (Adeoye et al., 2007), as the average microscopist can only detect 50 to 100 parasites per microliter (Payne, 1988). Reviewing peripheral blood smears is time-consuming (30 to 60 minutes) and requires a trained observer to interpret parasitemia, thereby limiting its capability for high-throughput screening. Inadequate staining and poor microscopy methods can degrade the visualization of the parasite making it more difficult for species differentiation.

Artifacts in blood can often be mistaken for malaria parasites even if proper staining techniques are performed (FIG. 1.11) (Sanofi Aventis, 2002). The most frequent mistake is the misidentification of platelets that are superimposed on red blood cells as malaria parasites. Their appearance is similar but platelets can be differentiated based on the

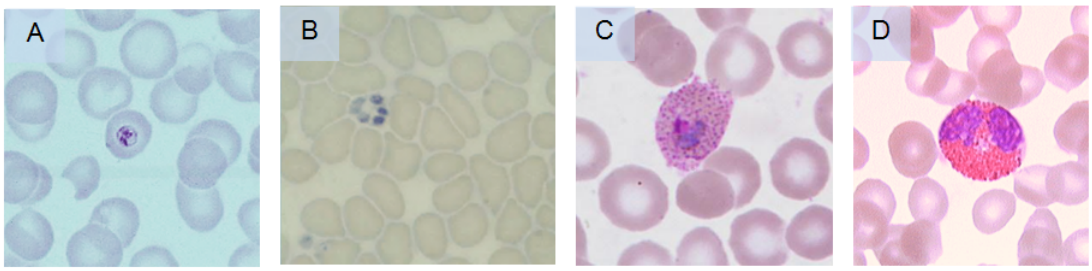

Figure 1.11: Interfering substances in peripheral blood smears. A. Platelet superimposed on a red blood cell. B. Platelet clump, which can potentially be misinterpreted as schizonts. C. Schüffners dots in a *P. ovale* trophozoite. D. Eosinophil, exhibiting red stippling in the cytoplasm similar to Schüffners dots. (Sanofi Aventis, 2002)

absence of chromatin dots and refringent patterns when focusing. Eosinophils can often be confused with *P. ovale* and *P. vivax* trophozoites because eosinophilic stippling is similar in appearance to Schüffners dots. Dust particles, stain deposits, obscuring debris, and blood cell ghosts are other common artifacts that may confuse the microscopist. Despite these insufficiencies, it is still the most common method for detecting *Plasmodium* parasites, with over 165 million peripheral smears performed in 2010 (Wilson, 2012).

1.8.2 Fluorescent Diagnostic Methods

Fluorescent stains such as acridine orange, DAPI, and benzothiocarboxypurine (BCP) have demonstrated efficacy in malaria diagnosis when conventional light microscopes are fixed with an interference filter. This method offers advantages particularly evident in conditions of low parasitemia. The rate of staining and observation is increased and the training level required to achieve consistent and reliable results is decreased. Excessive cost and availability of materials are limiting to these methods and a trained observer is still required for interpretation of results (Keiser et al., 2002; Kawamoto et al., 1992; Makler et al., 1991).

The nucleic-acid selective stain, acridine orange, has been successfully applied to the Quantitative Buffy Coat (QBC Diagnostics, Port Matilda, PA) system for rapid diagnosis of malaria and other parasitic infections with an eightfold increase in lower detection limits compared to Giemsa-stained thick smears (Adeoye et al., 2007). In this method, blood specimen is stained with acridine orange in a microhematocrit tube. After

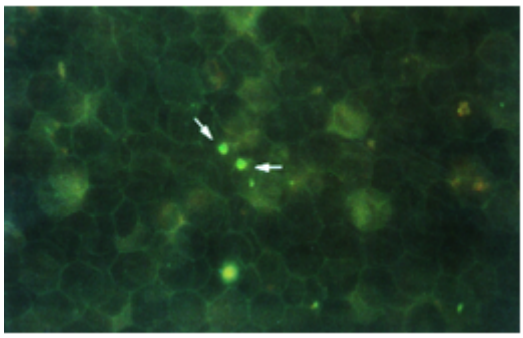

Figure 1.12: QBC Malaria test showing two trophozoites of *P. falciparum* (arrows). Parasitic DNA appears green and the cytoplasm appears yellow-orange. (QBC Diagnostics, 2012)

centrifugation, a clear plastic float, with a specific gravity equal to that of the buffy coat (WBC layer), settles to the buffy coat layer and expands this region up to ten-fold. RBCs infected with malarial parasites are less dense, and therefore occupy the space near the buffy coat - RBC interface. Centrifugal stratification concentrates the parasites into a discrete region (1 to 2 mm) and retains the parasites close to the tube wall so they may be visualized using a fluorescence microscope with an LED illumination attachment known as the ParaLens (QBC Diagnostics) (FIG. 1.12) (Estacio et al., 1993; Levine et al., 1989). Since the parasites are concentrated from a relatively large volume of blood ($\sim$ 50 to 110 µL, compared to $\sim$ 5 µL for peripheral smears), the sensitivity is increased and the examination time required to confirm or disprove infections is decreased. Levine et al. (1989) demonstrated that, after centrifugation is complete (5 minutes at 12,000 g), only 7 to 10 minutes are required for review to confirm that the sample is negative, and Estacio et al. (1993) demonstrated that less than one minute is required to confirm a positive infection.

The parasitemia magnitude can be approximated based on the number of parasites in a QBC field using the "Plus System", with assignments from +, which is the lowest parasitemia magnitude (i.e., <1 per field) to ++++, which is the highest parasitemia magnitude (i.e., >100 per field) (QBC Diagnostics, 2012). This manual computation aids in determining disease severity and monitoring the progress of patients under therapy.

Although the QBC significantly improves the sensitivity for *P. falciparum* detection, the specificity is compromised due to the staining of leukocyte DNA and numerous ar-

tifacts of stained acridine orange debris. Careful review by a trained morphologist is therefore still required for this method. Additionally, the specialized equipment required to separate the cell layers by centrifugation is relatively expensive (Adeoye et al. 2007; Tangpukdee et al. 2009).

Another fluorescent diagnostic method called the Partec Rapid Malaria Test (Partec, Münster, Germany) utilizes prepared borosilicate glass slides coated with fluorescent reagent to label malaria parasites (Partec, 2012). It has demonstrated equitable sensitivity, specificity, and a high level of agreement compared to Giemsa stain (Nkrumah et al., 2010). It is also cheaper (i.e., $0.50 per test compared to $1.00 for Giemsa), faster (i.e., 5 minutes per test compared to 25 minutes for Giemsa), and less labor intensive. Furthermore, the Partec CyScope microscope used to examine the specimen is capable of battery operation, providing a high degree of portability (Nkrumah et al., 2010). A trained observer is still required and other features, such as parasitemia computations and species differentiation, are difficult to achieve.

1.8.3 Rapid Diagnostic Tests

Rapid diagnostic tests (RDTs) offer a simple, prompt, accurate, and cost-effective diagnostic test for identifying malaria parasitemia by the detection of three distinct *Plasmodium* antigens. *Plasmodium* histidine-rich protein II (*p*HRP-2) is specific to *P. falciparum* and *P. Vivax*. *Plasmodium* lactate dehydrogenase (*p*LDH) is likewise specific to *P. falciparum* and *P. vivax*, but its isomers can also be used to detect all *Plasmodium* species (i.e., panspecific). Finally, *Plasmodium* aldolase is also panspecific. The combination of these antigens can be used to detect the presence of *P. falciparum*, *P. vivax*, or any combination thereof (Wilson, 2012). To perform a test, blood specimen is placed on a nitrocellulose strip with antibodies dispersed in well-defined lines (FIG. 1.13). The lysed specimen migrates down the strip and if it contains *Plasmodium* parasites, the complex of the antibodies and parasite antigens generates visible indicators to demonstrate a positive test result. A labeled goat antibody capture provides a control method to indicate that the test is functioning properly (Moody, 2002).

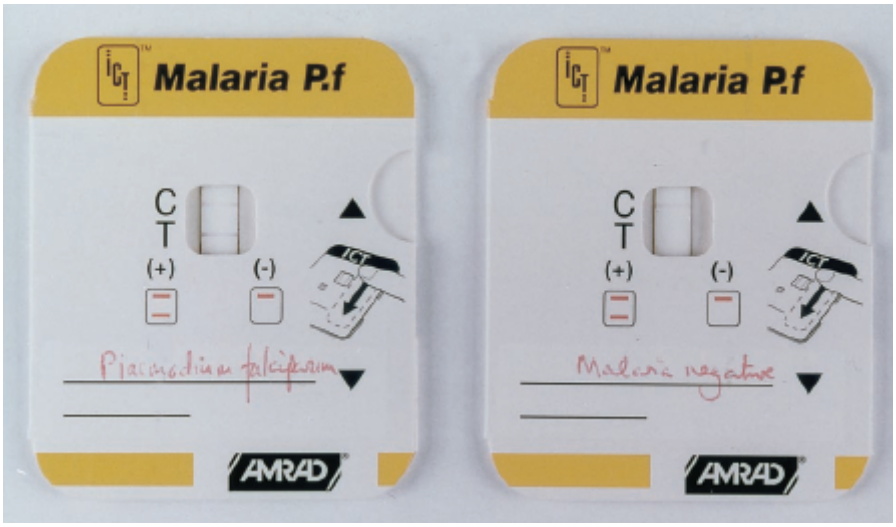

Figure 1.13: AMRAD (Sydney, Australia) rapid diagnostic test showing a positive result for *P. falciparum* (Left) and negative result (Right). (Moody, 2002)

Malaria diagnosis by RDTs has been reported as excellent (Tangpukdee et al., 2009), but there are several deficiencies with this method. First, non-*falciparum* infections may be misdiagnosed as negative for malaria if the RDT only contains *p*HRP-2. Multiple immunochromatographic tests must be combined when using RDTs to ensure that all species of malaria may be detected. There are also variants of *P. falciparum* in South America that do not produce HRP-2 and therefore cannot be detected using an RDT. Cross-reactions have been reported for patients with *Schistosoma mekongi* infection, rheumatoid factor or other auto-antibodies. Additionally, RDTs cannot be used to measure parasitemia magnitude, therefore the severity of the disease is not known to the clinician unless a peripheral smear is reviewed. Finally, RDTs are inefficient at diagnosing low parasitemia, which may lead to a false diagnosis and further symptom development by the patient. These limitations generally require the clinician to use RDTs in conjunction with other diagnostic methods for confirmation of reported results, characterization of infection, and to monitor the progress of patients undergoing anti-malarial treatment (Tangpukdee et al., 2009).

1.8.4 Polymerase Chain Reaction

Polymerase Chain Reaction (PCR) is a relatively new malaria diagnostic method that has been documented to be one of the most sensitive and specific tests especially in cases

of low parasitemia (Tangpukdee et al., 2009). It is common practice to utilize PCR as a confirmatory method in advanced laboratories due to its superior performance to Giemsa staining (Tangpukdee et al., 2009). Briefly, PCR is a process wherein the DNA of the parasite is amplified to several orders of magnitude greater. A process known as thermal cycling repeatedly heats and cools the sample to enable DNA melting and the subsequent enzymatic replication of the malaria DNA. PCR has demonstrated an ability to detect as little as five parasites per μL, or 0.001 % parasitemia, assuming a 5 x 10^6. It is important to note that the availability of PCR is limited in low wealth endemic regions due to its complex methodology, high cost, time-intensive procedure (i.e., >24 hours) and need for trained technicians (Tangpukdee et al., 2009; Moody, 2002). Quality control and regular maintenance is also a requirement of PCR, further limiting its potential for malaria diagnosis in rural areas. It is, therefore, mostly reserved for research and, occasionally, diagnostic purposes in large clinics and hospitals.

1.8.5 Alternative Diagnostic Methods

Other diagnostic methods such as serological, Loop-Mediated Isothermal PCR (LAMP), microarrays, flow cytometry, automated blood cell counters, and mass spectrophotometry are less commonly used. They each offer some distinct advantages but have significant limitations that diminish their effectiveness as malarial diagnostic methods.

1.9 Thesis Research Objectives

The imaging system, herein referred to as the Abbott Laboratories Imaging Platform (ALIP), is currently being developed by Abbott Laboratories for the point-of-care computation of complete blood counts. This technology is described in U.S. Patents 6,869,570, 7,903,241, 8,241,572, U.S. Patent Publications 2010/0216248, 2010/0273244, 2012/0021456, 2012/0219457, and U.S. Patent Application 13/630,934, among other published and pending patents (Levine et al., 2012a; Levine et al., 2012b; Wardlaw, 2002; Wardlaw, 2005; Wardlaw, 2010a; Wardlaw, 2010b; Wardlaw et al., 2011; Wardlaw, 2012; Verrant et al., 2012). The objective of this thesis was to develop a MATLAB (Math-

works, Natick, MA) algorithm to perform image processing techniques on a series of micrographs captured by the ALIP. In particular, the ALIP was used, but the image processing algorithms have universal application to other imaging modalities.

1.9.1 Sensitivity and Specificity

Girosi et al. (2006) categorized diagnostics instruments into three discrete levels in terms of infrastructure requirements (moderate, minimal, and no infrastructure), which ultimately determines their accessibility in low socioeconomic regions. The ALIP meets the criteria of moderate infrastructure primarily because electricity is required and battery operation is not yet possible (Girosi et al., 2006); however, because a trained technician is not essential to its operation, the ALIP may be considered as minimal infrastructure. Mathematical models by Rafael et al. (2006) demonstrate that a system of moderate infrastructure with 95% sensitivity and 95% specificity would save over 15,000 lives and avert over 141 million unnecessary malaria treatments each year and that a system of minimal infrastructure with 95% sensitivity and 95% specificity would save over 100,000 lives and avert over 390 million unnecessary malaria treatments each year. The clinical impact of this diagnostics system lies somewhere within this range, and therefore it was a goal of this research to develop an algorithm that is capable of diagnosing malaria with 95% sensitivity and 95% specificity to maximize its effectiveness regardless of accessibility limitations.

1.9.2 Auxiliary Functions

Another goal was the inclusion of features that offer novel information to help clinicians make an informed treatment decision. After a comprehensive literature review, several shortcomings of current technology were discovered, inspiring several clinically-useful functionalities made possible by the ALIP. These include the ability to automatically calculate parasitemia magnitude, differentiate erythrocytic stages, calculate infected red blood cell parameters, offer a method for blood transfusion screening, automatically transmit data to anyone in the world, and produce results in less than ten minutes.

1.9.3 Translation to Other Imaging Modalities

Although the algorithm was developed specially for the ALIP, it is also possible to apply this same process to other modalities, particularly those that utilize fluorescence microscopy. The application of an automated method for parasite detection would offer numerous advantages to existing technology, however, there are some translational limitations such as the requirement for low noise images without staining artifact that limit the application of such an algorithm to some modalities.

1.10 Comparison of "The Ideal Malarial Diagnostics System" and the ALIP

Malaria diagnostic systems should integrate accuracy, low cost, portability, durability and ease of use. Automation eliminates human error such as missed parasites in low parasitemia samples or fatigue that can occur during repeated Giemsa-stained slide review (Adeoye et al., 2007). As with any diagnostic test, sensitivity and specificity should be optimized to reduce the occurrence of false positives and false negatives.

Published in *Nature* in 2006, Rafael et al. suggest that

> "Tests should require no electricity or water, produce results in <5 min, rely on finger-prick blood, urine or saliva, and be entirely self-contained and simple to use and interpret, whether by healthcare workers with minimal training or for community or home use without training."

The ALIP does not require water, is capable of obtaining results in less than ten minutes, utilizes finger-prick blood, and is able to be used by minimally-trained technicians. The cost, portability, and electricity requirement limit its ability to be used in rural, resource-poor settings; however, the advantages of high sensitivity and specificity combined with numerous auxiliary functions and rapid turnaround time (TAT) offer significant beneficence to malaria diagnostics and offset its limitations.

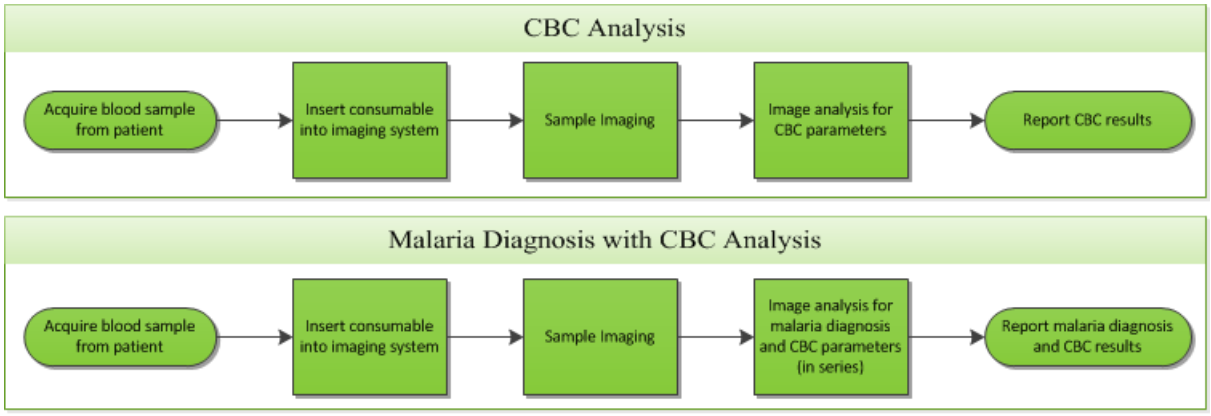

Figure 2.1: Existing infrastructure and algorithm (CBC Analysis) compared to new simultaneous malaria diagnosis and CBC (Malaria Diagnosis with CBC Analysis).

2 Methods

2.1 Overview of Imaging Platform

The Abbott Laboratories Imaging Platform (ALIP) is a unique technology that can offer significant advantages for malaria diagnosis. Briefly, this instrument uses an inexpensive consumable device (Verrant et al., 2012) to collect capillary or venous blood from the patient. Blood is mixed and processed within the consumable and then disposed on a proprietary imaging platform known as a chamber (Wardlaw, 2010a; Wardlaw, 2012). This chamber holds a quiescent sample of blood, which is then imaged in discrete regions by a programmable microscope (Wardlaw, 2005). Image processing techniques are then applied to diagnose malaria (Levine et al., 2012a).

It is important to note what instrumentation and software algorithms were available before the conduction of this research. The existing infrastructure and analysis algorithm is labeled in FIG 2.1 as CBC Analysis. The available CBC analysis algorithm was utilized throughout this research and a new malaria diagnosis algorithm was incorporated so that both a malaria diagnosis and CBC could be performed simultaneously (i.e., Malaria Diagnosis with CBC Analysis).

2.2 Biological Preparation

2.2.1 Specimen Acquisition and Preparation

Multiple *P. falciparum* cell culture strains including EG16 (sensitive), D6 (Chloroquine sensitive), W2 (chloroquine resistant), HB3 (chloroquine sensitive), 3D7 (wild type), Dd2 (chloroquine resistant), PfpmtD (knockout strain lacking PfPMT) and NF54 (sensitive) were provided by the department of Infectious Diseases at Yale New Haven Hospital (New Haven, CT). Peripheral smears were made by Yale research assistants before aliquoting to determine parasitemia level and stage development. It should be noted that human malaria samples were not available until later in the research process and therefore many of the developmental activities initially utilized cell culture. Both sample types have useful applications (i.e., human samples for patient diagnosis and cell culture samples for malarial research), and therefore both will be discussed in detail.

Babesia cell culture was also imaged to determine if it may likewise be detected by the prototype system. Infected *M. musculus* mouse blood samples mixed with K_2EDTA were provided by the department of Infectious Diseases at Yale-New Haven Hospital. The mice were RAG knockout because they do not exhibit an immune response to babesiosis, allowing high parasitemia levels to be achieved.

The hematocrit of all cell culture samples was modified to approximately 20% by removing cell media from the sample with a micropipette. This was accomplished by centrifuging the cell culture samples using a Plasmafuge 6 (The Drucker Company, Port Matilda, PA) to separate the packed red blood cells from cell media. A low centrifugal force (i.e., 500 g) and limited centrifugation time (i.e., 1 minute) prevented cell lysis in the samples.

To prepare the samples for image capture, cell culture was aspirated by pipette with acridine orange, trehalose dihydrate, and TX-305 solution (preparation methods discussed in Section 2.2.7). This method yielded optimal nucleic fluorescence and morphology of intraerythrocytic malaria and *Babesia* parasites.

Human malaria and *Babesia* samples were later provided by the Yale New Haven Hospital hematology department. All patient identification remained confidential. The

only revealed information was the classification of infection (i.e., malaria or Babesia) and the magnitude of parasitemia. Approval for clinical research was deemed unnecessary by the University of Connecticut Institutional Review Board due to compliance with the patient confidentiality standards set forth by the Health Insurance Portability and Accountability Act (HIPAA).

Human malaria samples were difficult to obtain due to the low prevalence of malaria in the United States. Samples are typically more common in the summer and early fall due to the reproduction of mosquitoes in endemic regions, but sample availability in the United States is limited to travelers returning from endemic regions. Samples could not be obtained from other resources due to patient confidentiality protection and sample degradation during transport. As a result, only one human malaria-infected sample was obtained; however, testing was performed in multiple replicates to extract as much data as possible.

Human negative control samples (i.e., blood samples not infected with malaria) were provided by Yale-New Haven Hospital and Yale-New Haven Shoreline Medical Center (Guilford, CT). A total of 44 human negative control samples from 22 patients were analyzed during the course of this research.

2.2.2 Infection Confirmation and Parasitemia Calculation Using Peripheral Smears

Prior to processing samples on the ALIP, the infection status was determined for each sample using standard microscopic examination protocol (Centers for Disease Control and Prevention, 2010a). It was imperative that a blind calculation of parasitemia be obtained so that peripheral smears could be used as a reference method to compare with the results of the algorithm. Sample identification was concealed and all microscopic calculations were performed prior to obtaining diagnostic results from the prototype. This method provided sufficient blinding to remove observer bias from parasitemia calculation *ex post facto*.

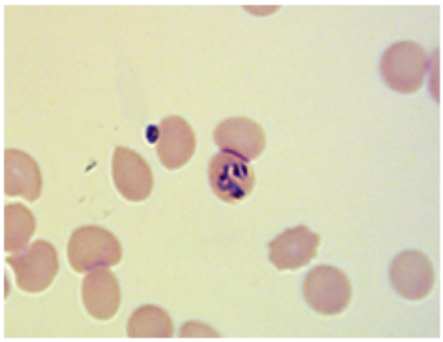

Figure 2.2: Wright-stained EG16 cell culture strain showing an early trophozoite and an extracellular merozoite. Image was captured on an Olympus BX41 microscope at 40X with oil immersion. Camera was an OptixCam Summit Series affixed to the extension tube of the microscope.

2.2.2.1 Giemsa Stain Preparation

Modified Giemsa stain solution was purchased from Sigma Aldrich (CAT No. 48900) and diluted 1:10 (v/v) in 1X PBS, resulting in a buffered-Giemsa solution with a pH of 7.5. The solution was then passed through No. 1 Whatman filter paper to remove extraneous debris, which can potentially induce artifact and interfere with manual diagnosis if the stain is not properly filtered.

2.2.2.2 Cell Culture Specimen Microscopic Examination

Giemsa-stained peripheral smears of cell culture samples were created at Yale University to confirm infection, calculate parasitemia, and determine stage development. Giemsa staining is considered the gold standard for parasitic detection; however, Wright's stain (Protocol Hema 3 Stat Pack, Fisher Healthcare) was initially utilized due to its availability. While it did not provide optimal coloration, intraerythrocytic parasites were nonetheless readily visible (FIG. 2.2).

2.2.2.3 Human Specimen Microscopic Examination

For human malaria and *Babesia* specimen obtained from the Yale New Haven Hospital Hematology Laboratory, Giemsa thick and thin blood peripheral smears were created for

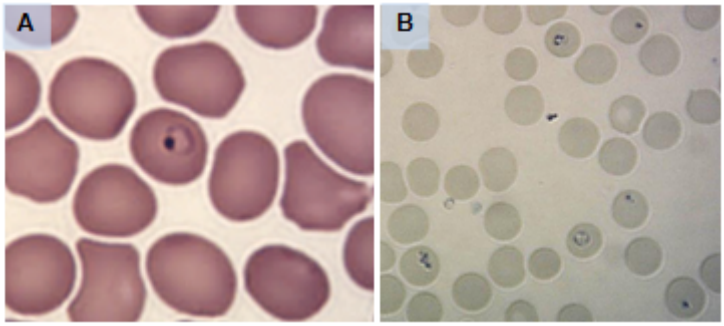

Figure 2.3: A. Human Wright-stained *P. falciparum* infected thin smear showing a single ring stage parasite. B. Human Giemsa-stained *Babesia* blood specimen showing multiple intraerythrocytic infections and extracellular merozoites with Giemsa stain. Images were captured on an Olympus BX41 microscope at 100X and 40X, respectively, with oil immersion. Camera was an OptixCam Summit Series.

each sample (FIG. 2.3) to confirm malarial infection and calculate parasitemia magnitude.

2.2.2.4 Microscopic Examination Protocol

In preparation of microscopic examination, peripheral smears were fixed in methanol for twenty seconds and allowed to air dry protected from dust. They were subsequently submerged in Giemsa stain for forty minutes, gently rinsed with distilled water, and allowed to air dry, again protected from dust. Smears were examined using a 40X objective lens (NA = 0.65) on an Olympus BX41 microscope with oil immersion covered with a No. 1 coverslip (VWR, Radnor, PA) to determine parasitemia magnitude. Species determination and qualitative observations were made with a 100X immersion objective (NA = 1.25).

Parasitemia in thin smears was calculated according to protocol set forth by the CDCs Laboratory Identification of Parasites of Public Health Concern (Centers for Disease Control and Prevention, 2010a), shown in Equation 5,

$$Parasitemia_{(thin\ smear)} = \frac{Number\ of\ infected\ RBCs}{Total\ number\ of\ RBCs\ counted} * 100. \quad (5)$$

A minimum of 10,000 RBCs were counted for each parasitemia calculation. RBCs with multiple intraerythrocytic infections were counted as one.

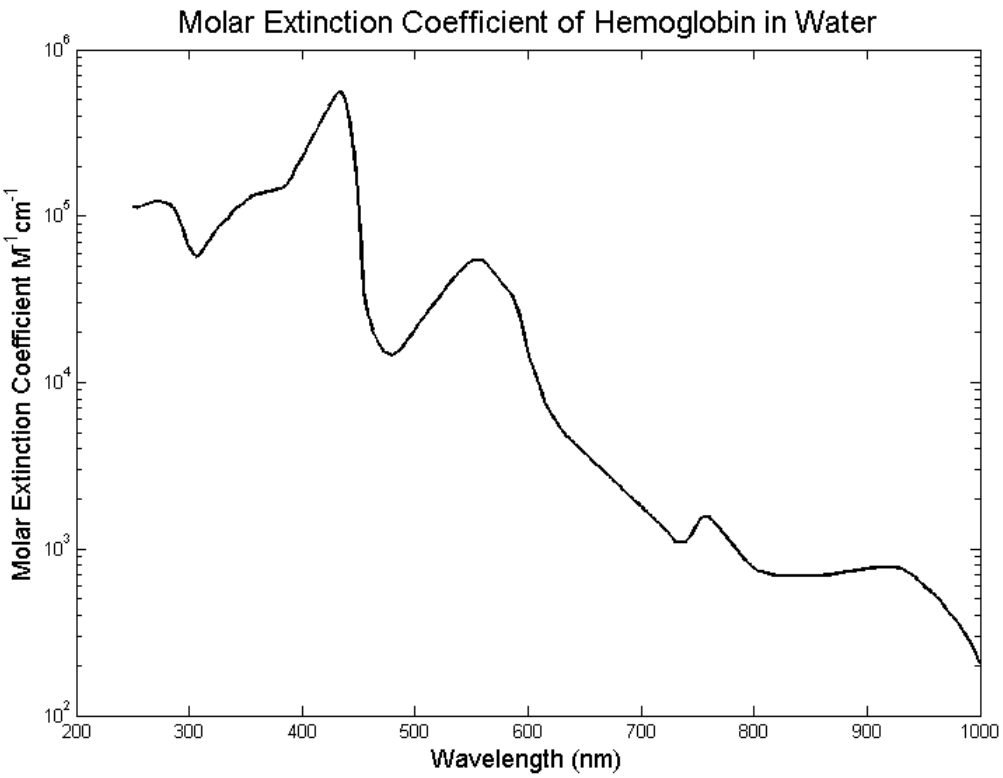

Figure 2.4: Absorption spectrum of hemoglobin (HGB) in water, expressed as molar extinction coefficient. (Prahl, 1999)

2.2.3 The Hemoglobin Light Absorption Spectrum

One of the most useful parameters employed in the prototype system takes advantage of hemoglobin's absorption spectrum. Hemoglobin (HGB) exhibits a molar extinction coefficient, ε, (i.e., measurement of how strongly a particular substance absorbs light at a given wavelength) from approximately 30,000 to 36,000 $cm^{-1}M^{-1}$ in the 410 to 415 nm light wavelength range (Horecker, 1942) as shown in FIG. 2.4. This peak absorption provides an optimal wavelength range for imaging.

RBCs were imaged by viewing their absorption, or optical density, using transillumination at 413 nm, as shown in the grayscale image of FIG. 2.5. This cell culture specimen is indicative of red blood cells in their natural morphological state (i.e., biconcave disk shape), as would be found within the human circulatory system. The dark region is the cell media and the gray-white objects are RBCs. It is important to note that areas of strong intensity (i.e., white) indicate an increased optical density of the 413 nm light, corresponding to a greater hemoglobin content. The central pallor, a region of reduced

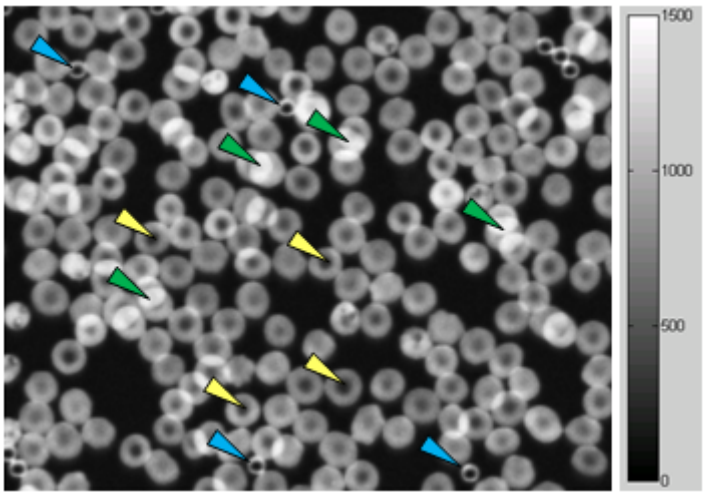

Figure 2.5: Grayscale optical density image (413 nm transillumination) of red blood cells in their natural morphological state. Specimen is a *P. falciparum* malaria cell culture. Yellow arrows indicate the central pallor, green arrows indicate overlapping cells and therefore increased optical density, blue arrows indicate beads. Color bar graphically illustrates the pixel values of the grayscale image between a dynamic range of 0 to 1500.

optical density due to the RBC's biconcave shape, is readily visible in non-sphered cells (yellow arrows). Some of the cells shown in the figure are overlapping, as indicated by an increased optical density in a localized region of the cell (green arrows).

It was difficult to determine the infectivity of cells in their morphological state because parasite visualization was limited. To enable detection, the sample must be mixed with an isovolumetric sphering agent, such as a zwitterionic detergent (i.e., zwittergent). When whole blood is thoroughly mixed with a sufficient concentration of zwittergent, the erythrocytic membrane contorts to form a relatively uniform spherical unit, facilitating intraerythrocytic parasite visualization as well as RBC indices calculations (FIG. 2.6) (Levine et al., 2012a; Wardlaw et al., 2011).

As described in U.S. Patent 7,903,241, zwittergent may deposited in a particular region of the chamber's interior to allow for both a region of sphered cells for intraerythrocytic parasite detection and RBC indices calculations as well as a region of non-sphered cells for qualitative RBC morphology assessment. Sphered red blood cells are shown in FIG. 2.7A using the same specimen as FIG. 2.5 but in a different region of the smear with a high concentration of sphered cells. FIG. 2.7B is a negative control specimen that was not infected with malaria.

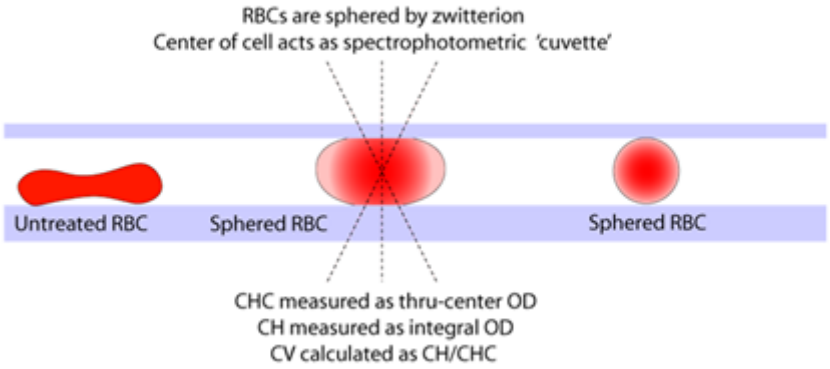

Figure 2.6: Isovolumetric sphering of red blood cells with zwittergent. Far left, untreated non-sphered RBC in its natural morphological state. Middle, macrocytic sphered RBC. Far right, microcytic sphered RBC.

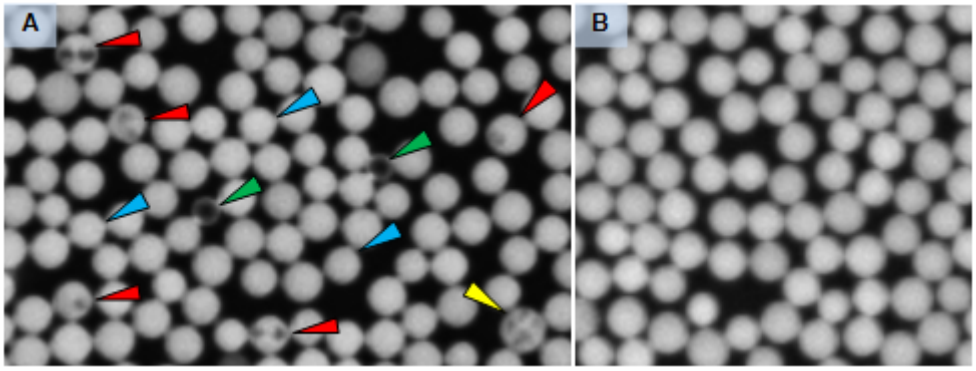

Figure 2.7: Sphered red blood cells using a zwitterionic detergent to facilitate intraerythrocytic parasite visualization and volumetric calculations. A. PY33A malarial-infected red blood cells with localized decrements (red arrows) due to displacement of hemoglobin by the intraerythrocytic parasite. Yellow arrow indicates a schizont with four distinct merozoites. Healthy (non-infected) cells are indicated by blue arrows. Beads are indicated by green arrows. B. Negative control sample showing an absence of localized decrements and a relatively uniform distribution of hemoglobin in all cells.

As shown in FIG. 2.7A, non-infected sphered RBCs exhibit a uniform distribution of hemoglobin (blue arrows); however, when infected with malaria, they exhibit a localized decrement of optical density (red arrows). This phenomenon occurs because the malarial parasite displaces hemoglobin throughout the cell and does not significantly absorb light at 413 nm (Levine et al., 2012a). The region in which the parasite resides is essentially void of hemoglobin and therefore the optical density is substantially reduced in this region.

2.2.4 Pre-sphering Zwittergent Solution Preparation

Although cell sphering is critical to the diagnosis of malaria, the sample chamber only spheres approximately twenty percent of RBCs within a sample. To select only sphered cells, an algorithm was developed in MATLAB to determine the extent to which each cell is sphered so that sphered cells can be differentiated from non-sphered cells.

It is preferential to sphere all RBCs in cell culture samples to maximize the number of cells that can be analyzed. This increases the lower limit of detection (LLOD) (i.e., the additional cells that could be analyzed would increase the chances of identifying intraerythrocytic parasites), particularly in samples with low parasitemia. The optimal zwittergent concentration for RBC sphering in cell culture was determined first, followed by optimizing the concentration in whole human blood.

Serial dilutions of zwittergent were created to determine the optimal concentration to sphere all red blood cells but limit cell lysis. When exposed to excessive amounts of zwittergent, the red blood cell membrane ruptured, releasing hemoglobin into the aqueous environment that caused a substantial reduction of intraerythrocytic optical density. It was important to limit the extent of cell lysis for a wide range of hematocrits because lysing decreased the intracellular parasite count and falsified other parameters during analysis. FIG. 2.8 displays a cell culture sample mixed with an excessive amount of zwittergent showing cell lysis (A), and an optimal concentration of zwittergent showing an absence of cell lysis and a complete sphering of all RBCs (B).

Sphering all RBCs in whole human blood will likewise increase the LLOD. An optimal zwittergent concentration was determined for whole human blood, which sphered all cells

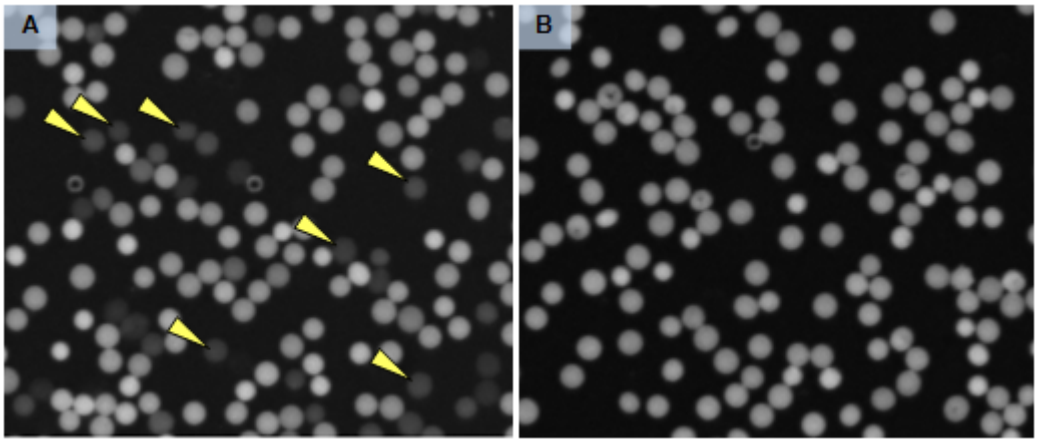

Figure 2.8: Pre-sphering with excessive zwittergent concentration and subsequent cell lysis (A) and optimal zwittergent concentration showing complete cell sphering (B).

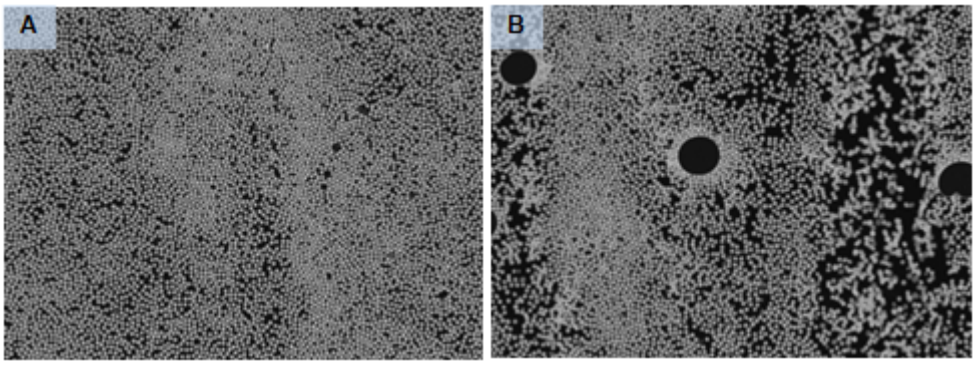

Figure 2.9: Cell pre-sphering using a malaria-specific consumable (A) and control consumable (B) in a negative control human specimen.

but did not induce cell lysis. This concentration was validated for a range of hematocrits from 10% to 60%.

Zwittergent solution was deposited within the consumable to mix with blood during consumable processing. This was validated through experimentation by directly comparing control consumables (i.e., no zwittergent) with zwittergent-coated consumables when whole human blood was processed (FIG. 2.9). All cells were sphered and no lysis was observed. A consumable with a zwittergent additive would therefore be easy to manufacture and implement for malaria diagnosis.

2.2.5 Acridine Orange Fluorescence Characteristics

When acridine orange (Invitrogen, Carlsbad, CA) is bound to DNA, it is characterized by an excitation maximum of 500 nm and an emission maximum of 526 nm (i.e., green in

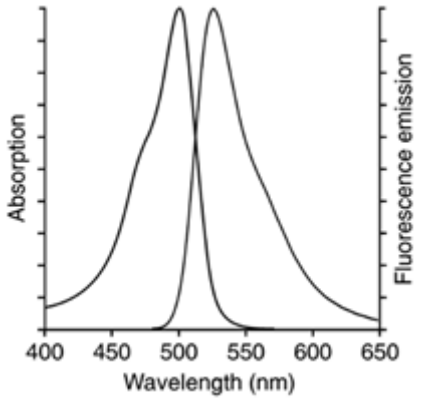

Figure 2.10: Absorption and fluorescence emission spectra of acridine orange when bound to DNA. (Life Technologies, 2012)

color) (Invitrogen, 2012). When bound to RNA, acridine orange is characterized by an excitation maximum of 460 nm and an emission maximum of 650 nm (i.e., red in color). The spectra of acridine orange bound to DNA is shown in FIG. 2.10 (RNA spectrum not shown).

The ALIP employs a 470 nm LED to take advantage of both excitation spectra so that both DNA and RNA fluorescent illumination can be captured with the same excitation wavelength. Alternating green and red filters allow for selectivity so that DNA fluorescence can be differentiated from RNA fluorescence (i.e., when the green filter is selected, only green fluorescence may pass through to the CCD camera, and vice versa).

Acridine orange is a useful fluorophore in imaging blood specimen because white blood cells (FIG. 2.11), platelets, and nucleated RBCs consist of both DNA and RNA. Other hematological components such as reticulocytes (i.e, immature RBCs) consist primarily of RNA.

2.2.6 Parasitic Fluorescence

In addition to the localized decrement of optical density, the fluorescent signature of the parasite can be used as confirmation for the presence of malaria (Levine et al., 2012a). The localized decrement caused by the displacement of hemoglobin by the intraerythrocytic parasite did not provide enough information to diagnose malaria on its own, particularly in human specimen where the optical density decrement was not as per-

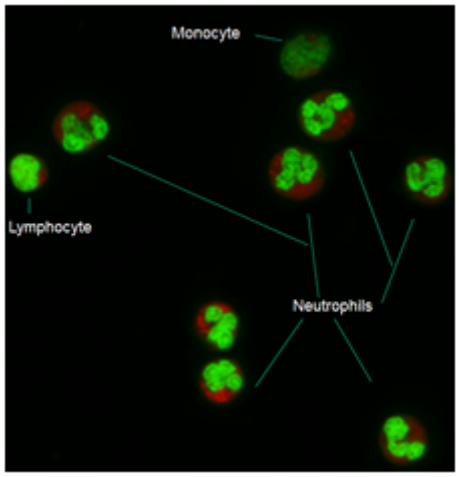

Figure 2.11: White blood cells imaged with the ALIP. The DNA of the nucleus and RNA of the cytoplasm fluoresce green and red, respectively, when bound with acridine orange.

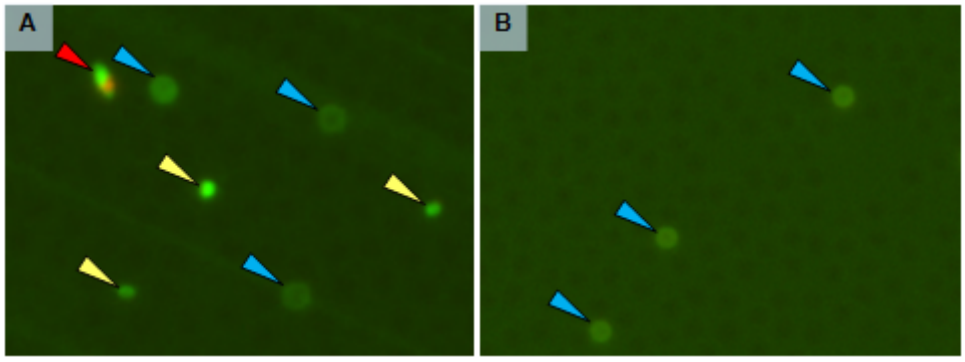

Figure 2.12: Parasitic fluorescence of three ring-stages (yellow arrows) and one gametocyte (red arrow) in a *Plasmodium falciparum* cell culture. Excitation at 470 nm optimizes the visualization of both DNA and RNA fluorescence. Beads are indicated by blue arrows. B. Negative control cell culture sample. Note in both images the absence of platelets and white blood cells.

ceptible as in cell culture. The staining characteristics of acridine orange are beneficial to the diagnosis of malaria by significantly improving both sensitivity and specificity.

Prior to being drawn into the disposable chamber, the sample is mixed with a solution of acridine orange, trehalose dihydrate, and Triton-X 305. As shown in FIG. 2.12, when excited at 470 nm, intraerythrocytic ring-stage parasites become readily visible and primarily fluoresce green with minimal red fluorescence. Gametocytes fluoresce green in an elongated crescent shape and also consist of a localized region of red fluorescence.

2.2.7 Acridine Orange Solution Preparation for Cell Culture Specimen

Since there were no WBCs or platelets present in cell culture samples, more acridine orange was available for parasitic binding, resulting in over-staining and saturation. An acridine orange solution formulation for cell culture was devised to optimize the staining morphology of malaria and *Babesia* parasites.

Serial dilutions of acridine orange were combined with trehalose dihydrate and TritonX-305. Trehalose dihydrate is a disaccharide used to prevent crystallization of the acridine orange when dried at room temperature, thereby improving it's solubility in cell culture or whole blood. Triton-X is a nonionic hydrophilic surfactant that improves the maneuverability of blood within both the chamber and consumable.

2.2.8 Interfering Substances

Some imaged objects have the potential to interfere with malaria diagnosis. These objects are known as interfering substances, and may be inherent to blood, internal within the chamber itself, or occur randomly. It was vitally important to classify interfering substances in order to remove them from consideration, thereby reducing the false positive rate.

2.2.8.1 Howell-Jolly Bodies

Some hematological conditions may be classified as interfering substances. For example, Holly-Jowell bodies, shown in FIG. 2.13B, exhibit a nuclear fluorescence similar to that of a malarial parasite; however, the fluorescent intensity of Howell-Jolly bodies is typically two times greater than malaria parasites. This difference in fluorescent intensity provided the primary method for differentiation (Levine et al., 2012a). Howell-Jolly bodies also do not exhibit a localized decrement of optical density, as shown in FIG. 2.13A (Levine et al., 2012a). It was therefore useful to observe the optical density of the suspected cell in addition to its fluorescence.

A clinical diagnosis should always be subsequently performed with any malarial diag-

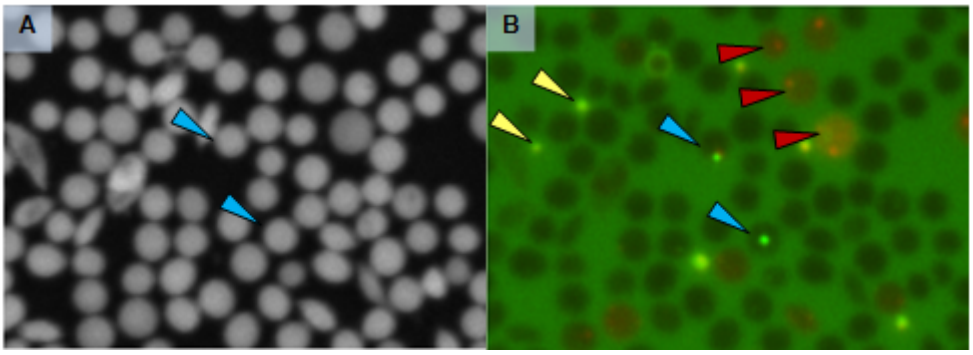

Figure 2.13: Howell Jolly Bodies (blue arrows) showing nuclear fluorescence but lack of localized optical density decrement. A. Optical density plane. B. Fluorescent plane. Howell-Jolly fluorescence indicated by small bright green region inside red blood cells. Two platelets (of six total) are indicated by yellow arrows. Three reticulocytes are indicated by red arrows. Reticulocytes consist of ribosmal RNA and therfore primarily fluoresce red. They pose no diagnostic interference to malaria.

nostics method to differentiate other benign conditions, such as the presence of Howell-Jolly bodies. The patient's symptoms, recent travel history, demographics, and medical history of splenic dysfunction or splenectomy should be considered. Howell-Jolly bodies are relatively rare in circulating blood and are typically caused by splenic hypofunction or asplenia (Sears et al., 2012). Howell-Jolly bodies can be easily differentiated from malarial infection when the appropriate clinical information is known or a peripheral blood smear is reviewed.

2.2.8.2 Babesiosis Differentiation

The Babesia parasite exhibits a fluorescent signature nearly identical to that of the *Plasmodium* parasite and also creates a localized decrement of optical density (FIG. 2.14). Differentiation between the two diseases using the relatively low-resolution images captured by the prototype system is difficult and, in some instances, may be impossible. Higher resolution images using improved optics (e.g., higher numerical aperture objective, at an increased manufacturing cost) may improve parasite visualization, but a clinical diagnosis should be performed to consider the patient's demographics and recent travel history to accurately distinguish the two infections. For example, if the patient lives in, or has recently visited, a malaria-endemic region such as Africa, the disease is likely to be

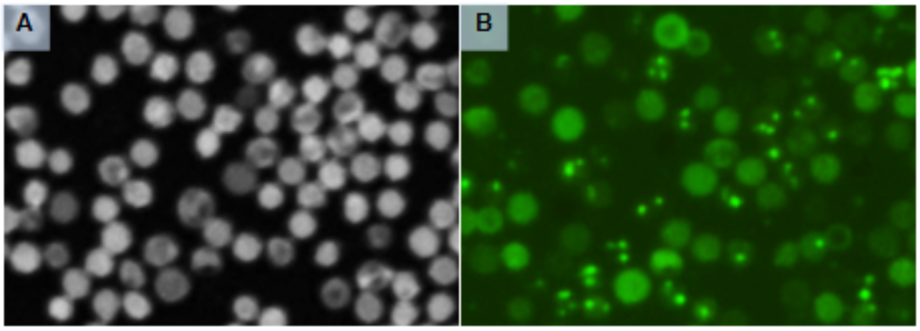

Figure 2.14: Babesia parasites in a 90% infected RAG knockout *M. musculus* mouse. A. Optical density channel showing similar morphological characteristics to Plasmodium infections. B. Fluorescence of the Babesia parasite.

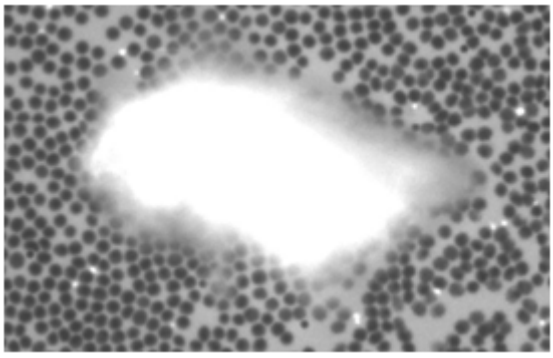

Figure 2.15: Green fluorescence of debris on the chamber surface (shown as grayscale).

malaria. Conversely, if the patient lives in, or has visited, a babesiosis-endemic region such as New England, then the disease is likely to be babesiosis. A Giemsa-stained peripheral smear should be reviewed to confirm the type of infection prior to drug administration.

2.2.8.3 Debris

Debris on the surface of the chamber, such as dust, also has the potential to interfere with malarial diagnosis. The anisotropic nature of such particles resulted in a significant reflection of the 470 nm light and high fluorescent intensity (FIG. 2.15). Under the right circumstances, this fluorescence could resemble a malaria parasite and generate one or more false positives.

In the same manner as debris, the edges of air bubbles within the chamber also fluoresce and have the potential to generate false positives (FIG. 2.16).

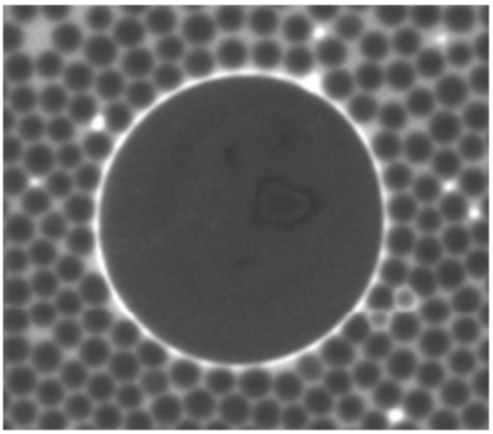

Figure 2.16: Green fluorescence of an air bubble (shown as grayscale).

2.3 Algorithm Development

2.3.1 Overview

The images obtained by the ALIP offer a plethora of information to enable a malaria diagnosis. The algorithm used to interpret these images to detect intraerythrocytic parasites and perform auxiliary functions using these images will be described. First, the structure and process of the algorithm will be described, followed by additional information that is particularly important for diagnosis.

MATLAB (ver. R2010b; Mathworks, Natick, MA) was used to process the micrographs of the ALIP because of its ease of implementation and expedient features. In future embodiments of the proposed system, other programming languages, such as C++, may be used to improve processing time.

FIG. 2.17 illustrates the variations between the CBC analysis and the malaria diagnosis + CBC analysis in the initial stages of image processing. In the case of the existing CBC analysis algorithm, the images were processed to determine the quantitative and qualitative parameters of the CBC. The Malaria Diagnosis + CBC Analysis utilized the same CBC algorithm, but also processed the images further to classify the malaria infection status of the specimen.

Masking is the first process used to determine the RBC locations within the images as well as remove or flag (i.e. alert the user) interfering substances. A total of three masks were created, including the RBC mask, debris mask, and NRBC mask. An exemplary

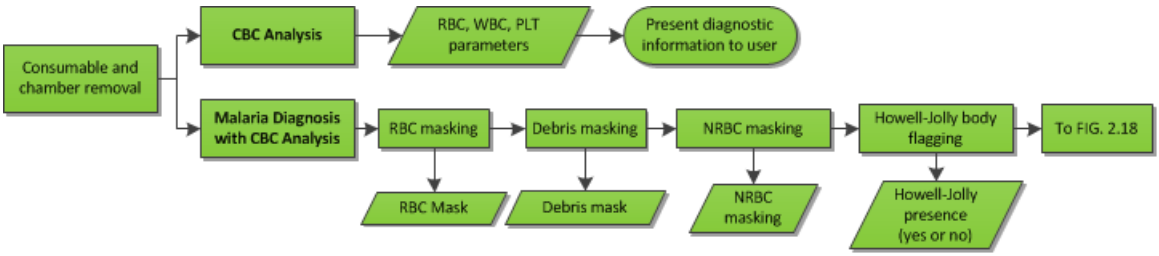

Figure 2.17: Analysis comparison following consumable processing and image capture. The malaria diagnosis actually occurs in series with the original CBC analysis algorithm.

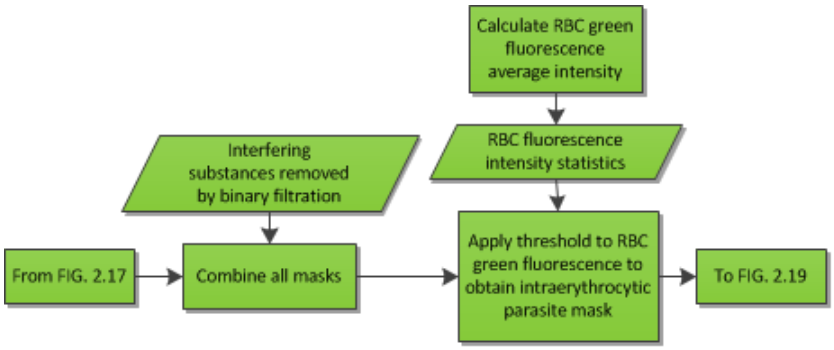

Figure 2.18: Mask combination and generation of intraerythrocytic parasite mask from RBC fluorescence characteristics.

RBC mask is shown in FIG. 2.21.

Next, all three masks were combined into one mask, ensuring that only the appropriate RBC regions were analyzed without any extraneous interference (FIG. 2.18). This combination mask may then be multiplied by the fluorescence or optical density images to obtain only fluorescence and optical density information for all masked RBCs, respectively. For example, if the mask is multiplied by the green fluorescence image, then only the green fluorescence of the RBCs was selected as a subset of the entire green fluorescence image, which also included fluorescence of WBCs, PLTs, and other cellular components.

The average RBC fluorescence intensity was calculated from the RBC-fluorescence-only image and was used to determine the appropriate threshold information to create the intraerythrocytic parasite mask. This mask may then be multiplied by the original green fluorescence image to obtain only the intraerythrocytic parasite green fluorescence.

The next stage of the algorithm was the decision as to whether or not a particular cell was infected with malaria (FIG. 2.19). Each cell within the RBC green fluorescence image was analyzed in series according to three decision criteria, including intensity, area

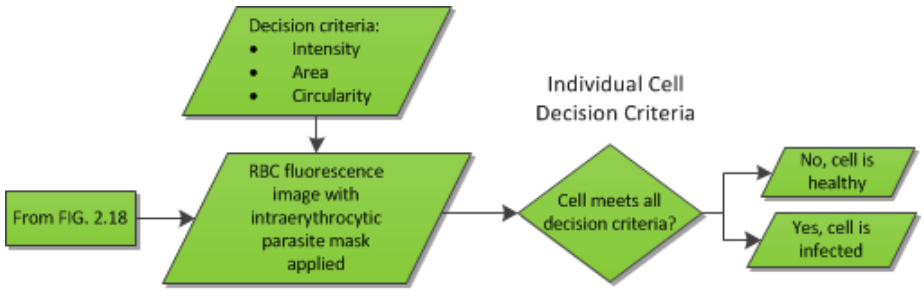

Figure 2.19: Individual cell decision criteria.

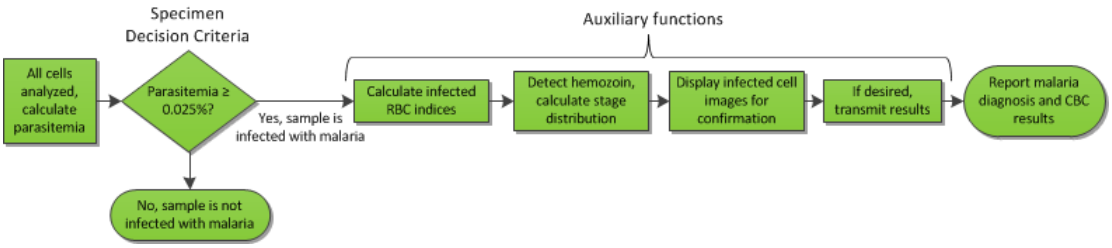

Figure 2.20: Sample decision criteria.

and circularity, which refer to the pixel values of the parasitic fluorescence. If a particular cell met all of the specified criteria, it was classified as infected, otherwise, it was classified as healthy.

Once all cells within the intraerythrocytic parasite green fluorescence image were analyzed, the next process was to finally classify the sample, as a whole, as infected or healthy (FIG. 2.20). The discrimination threshold was set so that if the calculated parasitemia of the sample was equal to or exceeded 0.025%, the sample was classified as infected, otherwise, the sample was classified as healthy. If the sample was classified as malarial infected, the algorithm continued to perform auxiliary functions on the images in series.

2.3.2 RBC Mask

Masking is a segmentation method used to identify particular objects within an image. A mask to identify sphered RBCs was required first because it defines the RBC's region of interest (ROI) in which all other analyses are performed.

Using MATLAB's inherent segmentation functions, a binary mask was constructed to identify red blood cells in each individual frame. There were 86 image frames in total, but

only 21 frames at the leading edge were sufficient for diagnosis. This is because red blood cells at the leading edge are mostly sphered by the zwittergent located in this region of the chamber. There are approximately five thousand RBCs per frame, depending on the patient's hematocrit, so an approximate total of 105,000 cells are capable of being analyzed. Therefore, this system is theoretically be capable of detecting one parasite in 105,000 RBCs (i.e., 0.00095% parasitemia), although this claim will need to be validated in human clinical trials with more developed algorithms that reduce the false positive rate. This is approximately the same LLOD as Giemsa thick smear review with an average microscopist. For comparison, the expected sensitivity of thick smears is 0.001% parasitemia (i.e., 50 parasites/μL, assuming a 5 x 10^6 RBC count), but most routine diagnostic tests typically achieve a sensitivity as low as 0.01% (i.e., 500 parasites/μL) (Tangpukdee et al., 2009; Moody, 2002).

It was important to only analyze RBCs that are spherical in nature and, therefore, an algorithm was developed to identify sphered RBCs. The RBC mask (FIG. 2.21) was created from a multistep process, including thresholding, watershed transform, erosion, circularity, and artifact removal. First, a preliminary mask was generated from the optical density image using an empirically-determined threshold based on collected statistics of RBC optical density. This mask correctly identified RBCs but was processed further in order to improve segmentation. A major issue was that an RBC in close proximity to another RBC (i.e., direct contact) would have overlapping optical density regions and the two RBCs may be considered as one object. To prevent this phenomenon from occurring, MATLAB's *watershed* transform using Fernard Meyer's flooding algorithm (Meyer, 1994) was applied to further segment the RBCs.

On occasion, the edges of RBCs that were proximal to a fluorescent object (e.g., WBC, platelet, debris, etc.) exhibited faint fluorescent illumination that could potentially interfere with diagnosis. To prevent this from occurring, the watershed mask was morphologically eroded to eliminate edge pixels that may contain fluorescence and extracellular artifact. Next, non-spherical objects were removed from the mask, as these objects were frequently RBCs in their natural biconcave shape. Each object's circularity,

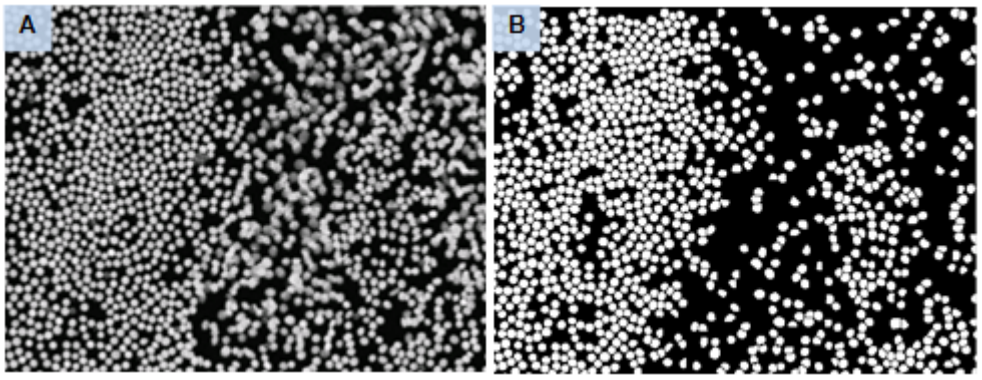

Figure 2.21: A. RBC image of optical density at 413 nm. B. Binary RBC mask.

or roundness, is given by

$$Circularity = \frac{4\pi * Area}{Perimeter^2}, \tag{6}$$

wherein MATLAB's *regionprops* function was used to obtain the pixel area and perimeter of each object in the RBC mask. Objects with a circularity below an empirically-determined threshold were removed from the mask. Finally, any objects that were too large or small were removed from consideration.

FIG 2.21 demonstrates that RBCs were successfully masked by these techniques. Note that the non-sphered cells were not selected during this process.

2.3.3 RBC Mask as a Binary Filter

The final RBC mask acted as a binary filter when multiplied by the red blood cell green fluorescence image so that fluorescence measurements could be performed within the defined regions of interest (i.e., only the intraerythrocytic fluorescence). Each object in the mask contained binary true values (i.e, 1 = true, RBC region; 0 = false, non-RBC region), so that when the mask was multiplied by the fluorescence image, the fluorescence pixel values of the RBCs were retained (FIG. 2.22).

This method defined only the RBCs as the ROI, thereby eliminating all plasma material including white blood cells and platelets from consideration. As previously discussed, it was impractical to differentiate between extracellular parasites and platelets using the proposed system due to their similar morphological appearance. This was not of much

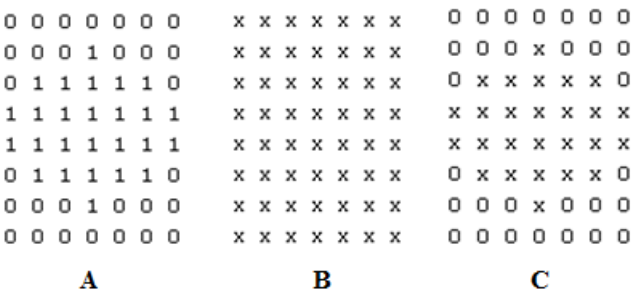

Figure 2.22: Binary mask filtration illustrated example. A. Identified RBC showing true values (logical 1) for the RBC region and false values (logical 0) that represent the extracellular region (e.g. plasma). B. Fluorescence image wherein each "x" represents some pixel value between 0 and 4095, representing the fluorescence intensity of that pixel. C. Binary mask applied from the multiplication of A and B. Each x multiplied by a true value results in a value of x, whereas each x multiplied by a false value results in a false value.

concern from a clinical standpoint because parasitemia calculations using standard microscopic review do not consider extracellular parasites. WBCs did not interfere with diagnosis due to their large pixel area and saturation of fluorescence illumination. The large size of WBCs (diameter often >10 μm, depending on type) also prevented them from migrating to the frames at the leading edge and restricted their locality proximal to the inlet port of the chamber. This acts as a natural filtration mechanism to further prevent WBCs from being considered in the analysis.

RBC fluorescence is shown in FIG. 2.23 after binary filtration, illustrating that the intraerythrocytic fluorescence information for each RBC was retained. The RBC mask can likewise be applied to the optical density image to obtain only RBC optical density.

2.3.4 Intraerythrocytic Parasite Mask in Cell Culture Specimen

Once the RBC mask was optimized and provided a suitable filtration means within the green fluorescence image, an algorithm was developed based on the information available in the various images. To classify a particular cell from a cell culture specimen as infected or uninfected, both the fluorescence and optical density images in the ROI were examined. To classify a cell from human specimen as infected or uninfected, only the RBC green fluorescence image (after binary filtration) was examined.

To determine the infectivity of an individual RBC in a cell culture specimen, the

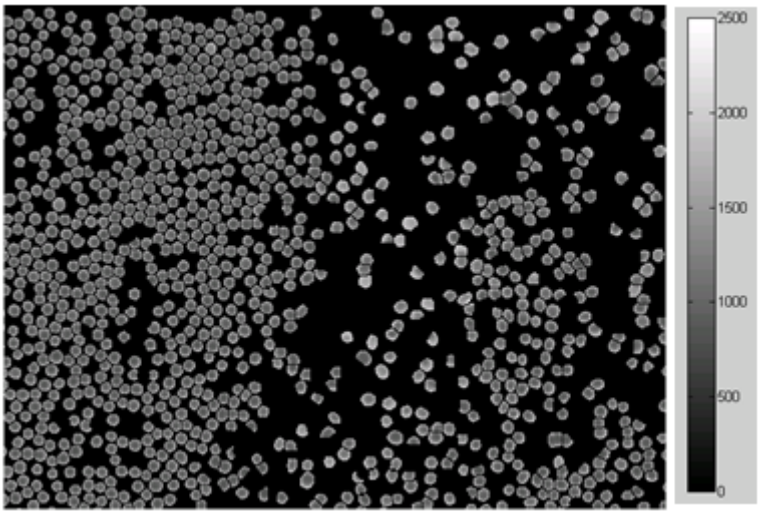

Figure 2.23: Intraerythrocytic fluorescence with binary filter applied, shown as a grayscale image with a dynamic range between 0 and 2500. All black regions are logical false values (0).

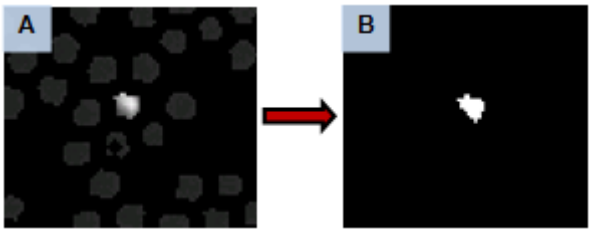

Figure 2.24: Interpretation of green fluorescence to determine infection status. A. Green fluorescence (grayscale image). B. Resulting mask due to green fluorescence exceeding the set threshold value.

green fluorescence and optical density were examined according to a set of predefined criteria. Each cell obtained from the RBC mask was analyzed one at a time within a for loop capable of analyzing 5,000 cells in approximately five seconds. The methods for intraerythrocytic parasite detection are described in U.S. Patent 13/630,934 (Levine et al., 2012a).

First, a threshold was applied to the green fluorescence of the RBC (FIG. 2.24A). All values exceeding this threshold were converted to logical true (FIG. 2.24B).

Next, the optical density of the cell was examined (FIG. 2.25). To determine if there was a localized decrement, the optical density of the parasite region (as determined by the mask of FIG. 2.24B) was compared to the optical density of the region that did not contain the parasite. If the average optical density of the parasite region was three

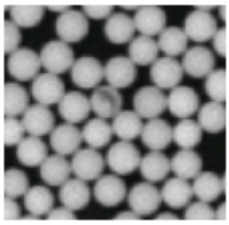

Figure 2.25: Interpretation of optical density to determine infection status (same cell as FIG. 2.24). Cell shown in center exhibits a localized decrement of optical density in the same location as its fluorescent illumination.

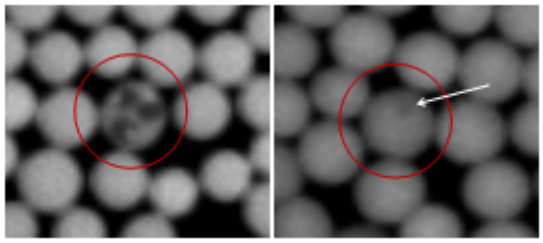

Figure 2.26: Comparison of localized decrement of optical density in cell culture and human specimen. A. Cell culture *P. falciparum* specimen showing schizont with three distinct intraerythrocytic merozoites each with a profound localized decrement of optical density. B. Human *P. falciparum* specimen showing single ring-stage parasite with a barely perceptible localized decrement

standard deviations below the average optical density of the non-parasite region, the cell was considered infected.

Because the cell of FIG. 2.25 exceeded the three standard deviation optical density threshold, it was classified as infected because it satisfied both the fluorescence and optical density criteria.

2.3.5 Intraerythrocytic Parasite Mask in Human Specimen

The human malarial sample only consisted of ring stage parasites, which exhibited a localized decrement that was significantly less pronounced compared to the cell culture specimen of FIG. 2.25.

It was determined that the localized decrement of ring stage parasites in human specimen did not contain enough information to be used as a criterion for infection (FIG. 2.26). For infection classification of human malaria specimen, the green fluorescence must therefore be further refined to distinguish malarial parasites from other interfering substances. To account for abnormal cells and artifact, the intraerythrocytic parasitic

fluorescence was further classified to consider the pixel area, circularity, and fluorescent intensity. Threshold values were determined from the typical parasitic characteristics shown in Table 1.

	Fluorescence Intensity	Area	Circularity
Average	1013.7	9.4	1.59
σ	140.9	2.4	0.21

Table 1: Parasite pixel value measurements (n=5,898 parasites) for green fluorescence intensity, area, and circularity.

Note that the average calculated parasitic circularity was greater than one. Theoretically, this is not possible because a perfect circle has a circularity equal to one. Circularities greater than one are resultant from *regionprops*' perimeter calculation as the line through the object's center. This erroneous phenomenon occurs on small objects, such as parasites. To correct for this, π may be added to the perimeter in the denominator,

$$Circularity = \frac{4\pi * Area}{(\pi + Perimeter)^2}, \tag{7}$$

which forces all small objects to have a circularity less than one; however, circularity measurements greater than one were still useful for differentiation because the relatively circular parasitic fluorescence exhibited a circularity much greater than the circularity of other interfering substances.

2.3.6 Detection of Hemozoin in Cell Culture Specimen

Hemozoin is produced throughout the entire malaria parasitic lifecycle but is only readily detectable in the later trophozoite and schizont stages. There are three methods to identify intraerythrocytic hemozoin using the ALIP (FIG. 2.27). These methods are described in detail by Levine et al. in U.S. Patent Application No. 13/630,934.

FIG. 2.27A depicts two distinct regions of a trophozoite that have an increased optical density at 413 nm relative to the rest of the cell. This is due to the fact that hemozoin is a dense, brown pigment that readily absorbs blue light. Since the parasite does not

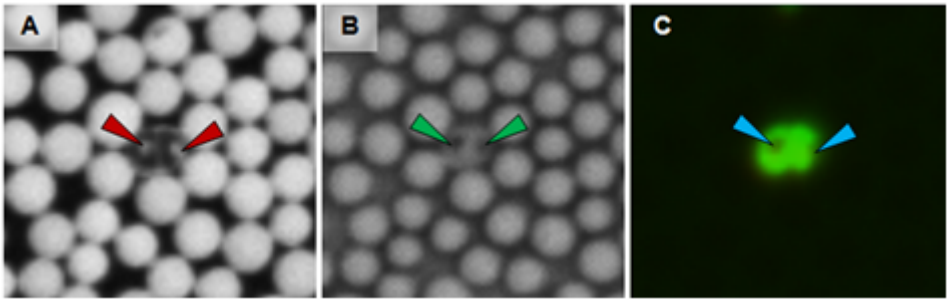

Figure 2.27: Detection of intraerythrocytic hemozoin in a *P. falciparum* infected cell culture. A. Optical density at 413 nm. Red arrows indicate the presence of hemozoin, manifesting as an increased optical density at 413 nm. B. Optical density at 660 nm. Green arrows show that the optical density of hemozoin at 660 nm is decreased relative to the other regions of the cell. C. Fluorescence illumination with 470 nm excitation. Blue arrows show that the hemozoin does not fluoresce.

absorb light at this wavelength, a localized decrement of increased optical density by the hemozoin (relative to the parasite's optical density) is readily visible.

FIG. 2.27B demonstrates that hemozoin absorbs less light at 660 nm than the remaining regions of the cell. Additionally, at this wavelength there is no observed localized decrement of optical density due to the parasite's displacement of hemoglobin; the absorption of 660 nm light by the parasite is therefore roughly equivalent to the optical density of hemoglobin at 660 nm.

Finally, FIG. 2.27C shows that hemozoin does not fluoresce when excited with a 470 nm LED. This is because hemozoin is comprised of crystallized heme and does not contain either DNA or RNA. Acridine orange will not accumulate in hemozoin.

Hemozoin can be readily detected by using a combination of all three images. This is especially important for *Plasmodium* stage differentiation and differentiation from other non-hematophagus intraerythrocytic parasites such as *Babesia*, which do not produce hemozoin.

2.3.7 Display Infection Message to User

Because the ALIP is primarily meant as a screening method, a message was only generated and displayed to the user in the event that malaria was actually detected. However, the system can be configured to present the information of a negative infection if desired. An example message is shown in FIG. 2.28 displaying the infection classification

Figure 2.28: Dialog box indicating the sample is infected with malaria.

and corresponding parasitemia magnitude.

Other diagnostic information is reported to the user but the most important parameters, namely the classification of infection and the parasitemia magnitude, is reported first in this alert message.

2.3.8 Auxiliary Functions

The flexible imaging technology of the prototype allows for many auxiliary functions to be performed that drastically improve the instrument's utility for malaria diagnostics. Some of the features developed during the course of this research will now be discussed in further detail.

2.3.8.1 Parasitemia Magnitude

The parasitemia magnitude, reported as a percentage, is given by

$$Parasitemia = \frac{Number\ of\ infected\ cells}{Number\ of\ analyzed\ cells} * 100. \tag{8}$$

This value was calculated from the cell-by-cell analysis and is subsequently displayed to the clinician for all samples that are considered to be infected with malaria. The ALIP is the first instrument capable of automatically calculating parasitemia magnitude; all other methods require time-intensive manual interpretation that can take up to 60 minutes or more.

The parasitemia magnitude is a vitally important parameter to know when treating a malaria patient because it indicates the disease severity of the infection. For example, a patient with 1% infected cells must be treated more aggressively than a patent with

0.01% infected cells.

2.3.8.2 Calculation of Infected-RBC Indices

The RBC indices include mean cell hemoglobin (MCH), mean cell hemoglobin concentration (MCHC), and mean cell volume (MCV). MCH is a measure of the average mass of hemoglobin in RBCs, MCHC is a measure of the concentration of hemoglobin in a given volume of packed RBCs, and MCV is a measure of the average cellular volume of RBCs. These parameters, reported in a standard CBC, are often useful in differentiating types of anemia.

The ALIP also allows the RBC indices to be calculated for each infected RBC. This feature is unavailable in any current technology and can be utilized to evaluate *in vitro* or *in vivo* drug efficacy, monitor a patient's progress with drug treatment, evaluate a patient's response and resistance to a particular drug, aid researchers in developing novel candidate drugs, and other clinically-beneficial applications.

Once a particular cell is classified as infected, its hemoglobin content, hemoglobin concentration, and cell volume may be computed according to the methods discussed in U.S. Patent 2009/0238438 (Wardlaw et al., 2011). Briefly, the hemoglobin concentration is determined by examining the optical density of a portion of the RBC in accordance with the Beer-Lambert Law,

$$OD = \epsilon c L \tag{9}$$

where ε is the hemoglobin molar extinction coefficient, c is the hemoglobin concentration, and L is the distance traveled through the RBC. Since ε and the pathlength are known quantities and the OD may be computed from the particular region of the cell, Equation 9 can be rearranged to solve for the hemoglobin concentration, c. With a known hemoglobin concentration, all RBC indices may be computed by averaging the plurality of cell-by-cell data.

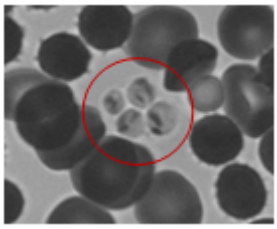

Figure 2.29: *P. falciparum* cell culture showing four distinct merozoites. High resolution 413 nm transmission image using a 100X objective and immersion oil.

2.3.8.3 Improvements to Resolution and Parasitic Visualization

The optical resolution of the prototype system was sufficient to determine CBC parameters, identify malarial infection, and enable auxiliary malarial functions to be performed, but it was intentionally kept relatively low to reduce the overall cost of the optical components. Although acridine orange fluorescence is limited in its ability to morphologically distinguish parasites, higher resolution optics would improve parasitic visualization and possibly allow for *Plasmodium* species differentiation. This would need to be verified with alternative hardware integration, but it may not be necessary because clinicians will likely prefer to examine peripheral smears with a microscope if any detailed parasite morphology information is required. An exemplary high resolution transmission image obtained by the prototype system is shown in FIG. 2.29.

2.3.8.4 Transmission of infected RBC images via Simple Mail Transfer Protocol

MATLAB's *sendmail* function allows messages and attachments to be sent to a list of recipients using Simple Mail Transfer Protocol (SMTP). If the user requests that the images are to be reviewed by an expert malariologist somewhere in the world, the prototype system can manually or automatically (based on user preference) send data with a wired or wireless internet connection. Transmitting patient information should always comply with HIPAA, so patient identifiers can be omitted if necessary. If the appropriate settings are selected, a dialog box will automatically be presented to the user when an infected sample is detected (FIG. 2.30). The user may also manually select to

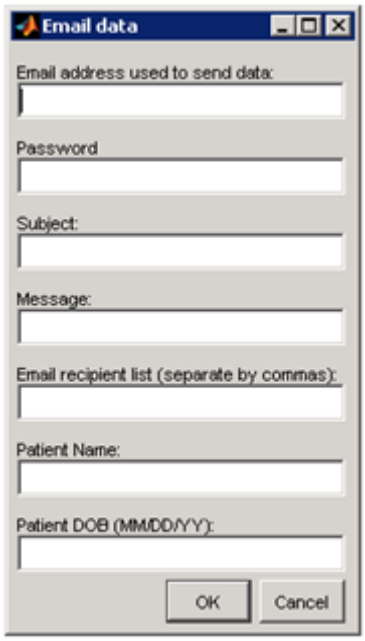

Figure 2.30: Dialog box requesting recipient list to email data.

send data after the analysis has been performed.

A valid email address must be entered in order to send data via email. The program currently uses the Gmail servers to send email with a Secured Sockets Layer (SSL) encryption. Depending on the email web host, other authentication and encrypted connections may be required.

A cell variable is created to contain the images of infected cells stored in a portable networks graphics (.png) file as well as diagnostic information stored in a comma separated values file (.csv). Testing of the SMTP feature resulted in the transmission and reception of the email in less than ten seconds on average.

If the user wishes to recall data from a previous session, data may also be saved to a local or external hard drive. This functionality is accomplished in a similar manner by using the *saveas* MATLAB function. The user is prompted to select a destination folder and all images and diagnostic data is saved to the specified directory with necessary patient information.

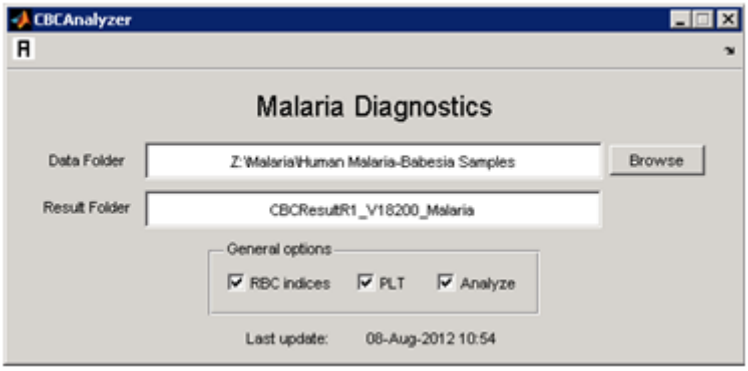

Figure 2.31: Graphical user interface for the MATLAB malaria diagnostics algorithm.

2.3.9 MATLAB Graphical User Interface

The graphical user interface (GUI), shown in FIG. 2.31, allows the user to select a 'Data Folder' with imaged samples and output all diagnostic data to a specified 'Result Folder' in the same parent directory. Once the appropriate folders are selected, the user simply selects the capital 'A' in the upper left-hand corner to start the program. The most recent update date and time is shown to indicate the current program version.

In the final commercialized product, this GUI will not be available to the user. Instead, the system would analyze the samples automatically following a completed imaging sequence. It was created for research purposes only using MATLAB's interactive *GUIDE* tool.

2.4 Receiver Operator Characteristic Curves

The Receiver Operator Character (ROC) curve provides a useful means to assess the diagnostic accuracy of a test. This signal detection statistical measure was originally developed during World War II to interpret radar signals for the differentiation between flocks of birds and enemy aircraft. Today, it is commonly applied to medical diagnostics for the binary classification of disease positives or negatives within a bimodal distribution (FIG. 2.32) (Fawcett, 2006). It was useful to generate a ROC curve to aid in determining the optimal threshold for infection classification; a threshold was selected due to its balance of sensitivity, specificity, and LLOD.

FIG. 2.32 displays a theoretical distribution of two populations that either have the

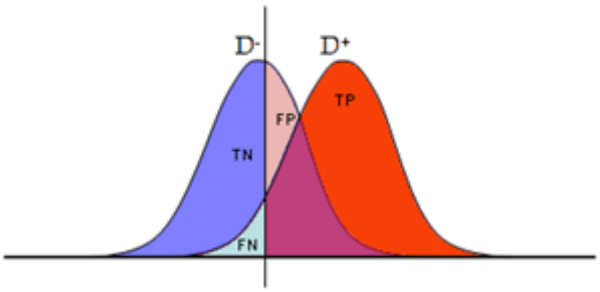

Figure 2.32: Bimodal distribution of a population with the disease (D^+) and a population without the disease (D^-). (Wikipedia, 2006; modified and reproduced under the terms of the GNU Free Documentation License)

disease (e.g. malaria) (D^+) or do not have the disease (D^-). The abscissa of FIG. 2.32 in general represents some test value. In this case, the test value is the calculated parasitemia value.

An empirically-derived threshold represented in the figure by a black vertical line defines the true positive (TP), true negative (TN), false positive (FP), and false negative (FN) rates. Moving the threshold to the right along the abscissa, for example, would increase the specificity but decrease the sensitivity. The dichotomic tradeoff between sensitivity and specificity depends on the particular application, specifically which criterion contributes more to a positive outcome. Airport security, for example, favors sensitivity over specificity to ensure that all potentially hazardous material is detected. Malaria diagnostics requires a balance between sensitivity and specificity. Higher levels of detection (i.e. sensitivity) allows for early detection and ultimately contributes to decreased mortality rates (Rafael et al., 2006). Highly-specific tests contribute to a decreased consumption of antimalarial drugs in resource-poor regions for patients that do not have malaria, thereby decreasing unnecessary treatments and resource waste.

3 Results

3.1 Sensitivity and Specificity Analysis

In order to determine the diagnostic efficacy of the proposed algorithm, the sensitivity, specificity, PPV, and NPV were determined after analysis on human blood specimen. It is important to note that sensitivity and specificity of the ALIP were initially measured on a cell-by-cell basis (i.e., each individual cell was examined and the algorithm interprets whether or not that cell was infected with malaria). This was referred to as the "Cell-by-Cell sensitivity/specificity". The final measure of sensitivity and specificity was the binary classification as to whether or not each sample (i.e., patient) was infected with malaria. This was referred to as the "Sample-by-Sample sensitivity/specificity".

For human negative control specimen, the algorithm flagged an average of five false positives per sample, typically resultant from the interfering substances discussed in Section 2.2.8. To account for this, the lower cutoff of detection was set to a parasitemia of 0.025%, which provided a balance of sensitivity, specificity, and LLOD. Therefore, any sample with a calculated parasitemia magnitude less than 0.025% would be automatically classified as negative for malaria. Any sample with a calculated parasitemia magnitude greater than 0.025% would be classified as malarial-infected, and a message would be displayed to the clinician. Assuming an RBC count of 5 x 10^6/μL, a cutoff of 0.025% allows detection of 1,250 parasites/μL. This is comparable to the LLOD of gold-standard Giesma thick film review, which is routinely able to detect as low as 0.01% parasitemia, or 500 parasites/μL. Subtracting the background "noise parasitemia" (i.e., false positives) reduces the overall sensitivity and LLOD of the system but allows for some flexibility in regards to specificity. Because malaria parasitemia typically ranges from 0.001% to 0.1% or greater (Moody, 2002), a cutoff of 0.025% will sufficiently identify higher parasitemia infections. Of course, future improvements can be made to the algorithm that will decrease the occurrence of false positives and enable an even lower detection limit.

3.1.1 Cell-by-Cell Specificity

To determine the cell-by-cell specificity of the system, a total of 44 human negative control samples from 22 patients were analyzed by the prototype algorithm. All samples were confirmed negative by peripheral smear review of at least 10,000 RBCs (approximately 40 monolayer cell fields using a 100X objective with oil immersion). As a result, each time the algorithm classified a particular cell as being infected with malaria, it was known to be a false positive. This made for a straightforward analysis of specificity, the data of which is shown in Table 2.

Samples Analyzed	Cells Analyzed	True Negatives	False Positives	Specificity
44	2,360,701	2,360,470	231	99.99%

Table 2: Cell-by-Cell specificity data for human negative control samples.

3.1.2 Sample-by-Sample Specificity

The average "noise parasitemia" per sample was calculated as 0.00978% $\pm$ 0.0065% (i.e. on average, a sample's parasitemia was less than 0.01%). Only one of the 44 negative control samples had a calculated parasitemia greater than 0.025%, making it falsely classified as malaria-infected. The specificity of the algorithm on a sample-by-sample basis was therefore 97.7%, making it one of the more specific test methods currently available for malaria diagnostics.

3.1.3 Cell-by-Cell Sensitivity

To determine the cell-by-cell sensitivity of the algorithm, each cell had to be manually classified as infected or uninfected and then verified with the results of the algorithm. Both the green fluorescence and the optical density were viewed to manually determine the infection status. Cells were analyzed in sets of 100, as shown in FIG. 3.1. Due to the time-intensive nature of this evaluation, 5 human malarial-positive samples from the 1 infected patient were analyzed, with over 50,000 cells examined during the manual review.

To ensure that the manual analysis was sufficiently blinded, an unlabeled set of all

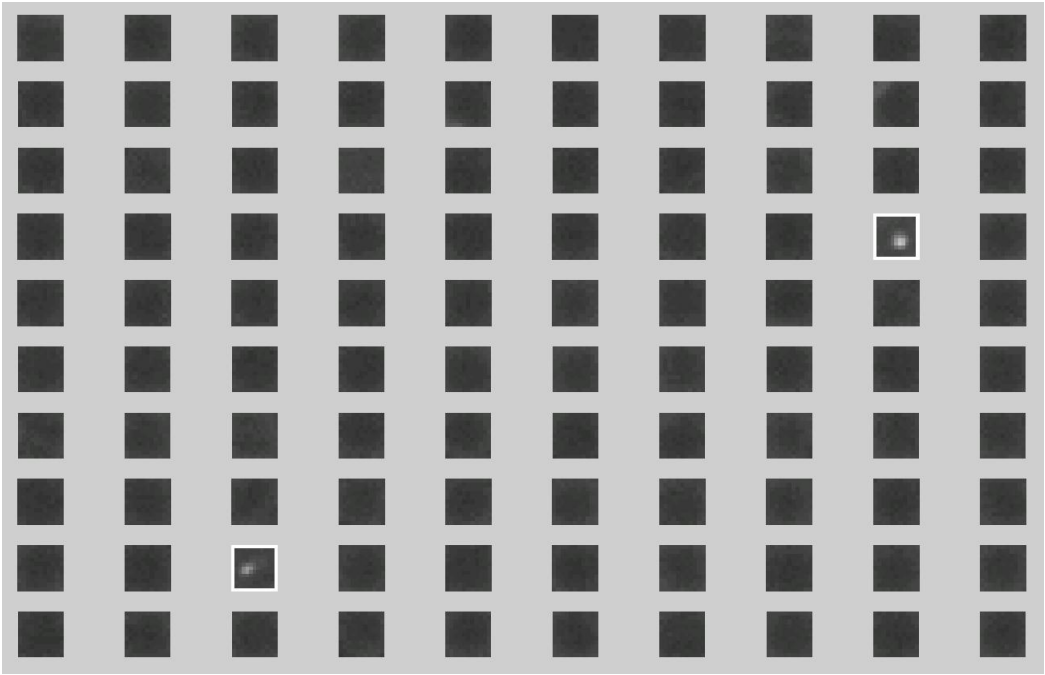

Figure 3.1: Labeled green fluorescence (grayscale image) of 100 cells to manually determine cell infection status. A white border around the cell indicates that the algorithm classified that particular cell as infected. In this set of 100 cells, for example, there were 2 true positives, 0 false positives, 98 true negatives, and 0 false negatives.

100 cells was displayed for analysis. Each cell was denoted as infected or uninfected and then subsequently verified with the labeled set of 100 cells shown in FIG. 3.1, which represents the algorithm's interpretation of the specimen. True positives, false positives, true negatives, and false positives were noted for each set. Data was compiled for a total of five samples of the fifteen total available samples(Table 3).

Samples Analyzed	Cells Analyzed	True Positives	False Positives	True Negatives	False Negatives
5	54,000	142	1	53,831	26
	Sensitivity	Specificity	PPV	NPV	
	84.5%	99.998%	99.3%	99.9%	

Table 3: Subset of cell-by-cell sensitivity data for human malarial-positive samples.

3.1.4 Sample-by-Sample Sensitivity

The parasitemia of all 15 samples was calculated by the algorithm as 0.32%, and therefore all samples were correctly classified as infected (sensitivity = 100%), since 0.32%>>0.025%. The actual parasitemia of this sample determined by Giemsa peripheral smear review was 0.45%.

3.1.5 Sensitivity/Specificity Summary

In summary, the patient specificity (sample-by-sample basis, n=22 subjects, 44 samples) was 97.7%. The patient sensitivity (n=1 subject, 15 samples) was 100%. The PPV and NPV were 93.8% and 100%, respectively. If a baseline 0.025% cutoff is used, the ALIP will not be able to detect malarial specimen with a parasitemia that is less than this threshold. This can be adjusted depending on sensitivity and specificity requirements. Receiver Operator Characteristic curves aid in the determination of discrimination thresholds.

3.2 Generation of the Receiver Operator Characteristic Curve

The discrimination threshold of the ALIP, or final decision criterion, for whether or not a sample is infected with malaria, depends on the calculated parasitemia. FIG. 3.2 displays the ROC curve for various parasitemia threshold levels ranging from 0.005% to 0.35%. Each data point (black squares) represents a specific threshold level. The data of FIG. 3.2 is modeled from the set of 15 malaria-infected samples and 44 negative control samples. In this graph, the abscissa represents the false positive rate (FPR), or one minus the specificity, and the ordinate represents the true positive rate (TPR), or sensitivity.

The area under the curve (AUC) of an ROC provides a summary measure of the diagnostic accuracy of a binary classification test (i.e., the greater the AUC, the more accurate the test is). Since random guessing produces a diagonal line from (0,0) to (1,1) (shown as a green line in FIG. 3.2), all diagnostic tests should have an AUC greater than 0.5. The AUC of this particular method of using parasitemia as the discrimination threshold gave an AUC of 1.0. Based on the ROC curve, a lower level threshold of 0.025%

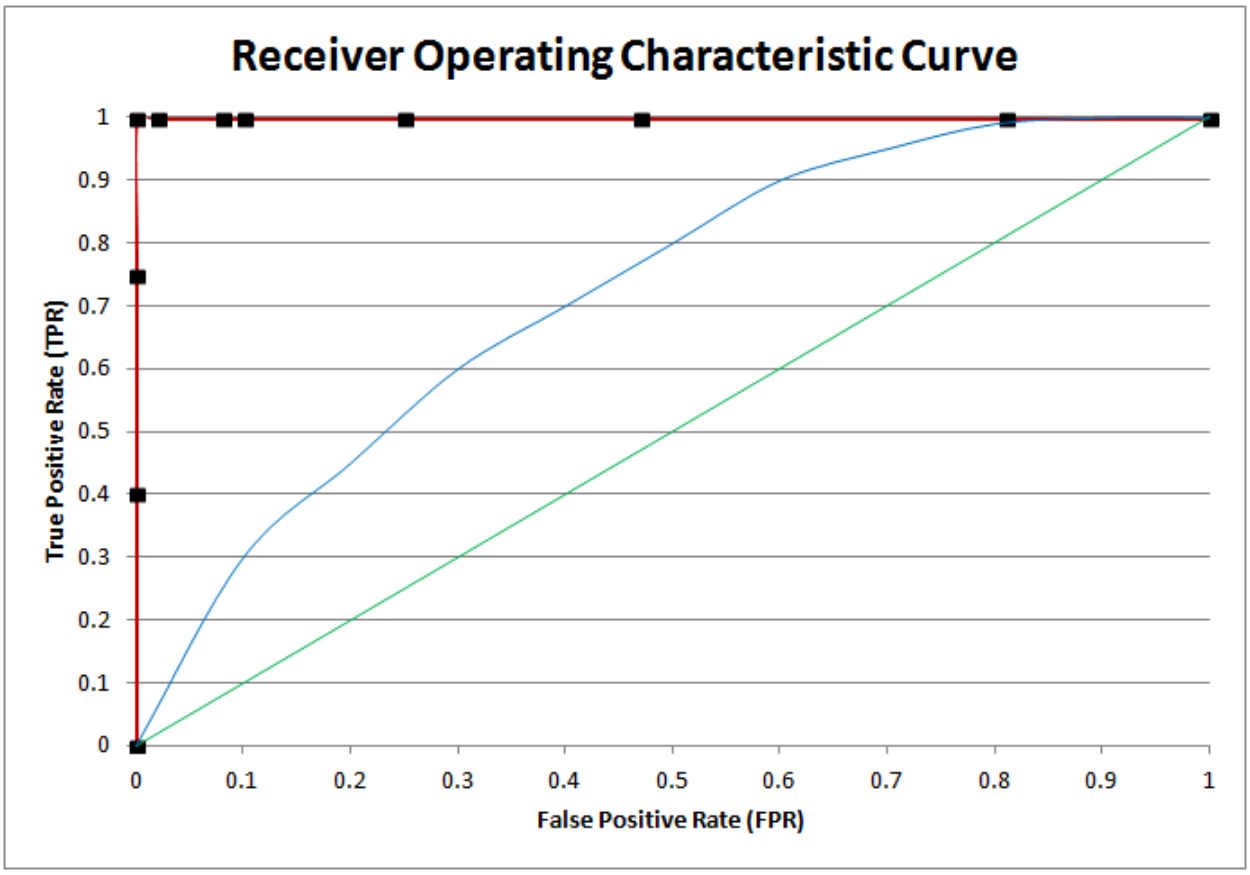

Figure 3.2: Receiver Operating Characteristic Curve (red line) of the image analysis algorithm using parasitemia as the discrimination threshold for sample infection. For reference, the green line shows a theoretical test using random guessing and the blue line shows the shape of a typical ROC curve for a diagnostic test

was chosen. This cutoff provided a balanced LLOD, sensitivity (100%), and specificity (97.7%), satisfying the goals of this thesis set forth in Section 1.9.1.

As discussed in the "Future Research" section of this thesis (Section 4.9.4), additional malaria-infected samples, particularly those with low parasitemia, should be analyzed to increase the statistical power of this analysis.

3.3 Calculation of Infected RBC Indices

The MCH, MCHC, and MCV were calculated from the plurality of 48,100 healthy, uninfected cells and the plurality of 145 infected cells (Table 4) in a human malaria infected specimen.

	MCH (pg)	MCHC (g/dL)	MCV (fL)
Infected (n=145 cells)	30.4	35.2	86.4
Healthy (n=48,100 cells)	29.3	35.7	83.6
p-value	0.0015	0.0049	0.0138

Table 4: RBC indices calculation for a malarial-infected human sample. p-values were calculated assuming a paired two-tailed distribution (α=0.05).

Notably, the MCH of infected RBCs was actually slightly higher than that of healthy, uninfected RBCs. The MCHC was slightly lower in infected RBCs, and the MCV was slightly higher in infected RBCs. All mean differences were significant ($p < 0.05$ for each index).

It should be noted that the analyzed sample was only comprised of ring-stage parasites. This early intraerythrocytic stage did not contribute to a significant decrement of hemoglobin and therefore a substantial decrease in hemoglobin content was not expected. Late stage trophozoites and schizonts are expected to contribute to a significantly lower MCH and MCHC. The increase in cell volume is expected due to the inclusion of the single ring-stage merozoite.

4 Discussion

The overall goal of this thesis was to develop an interpretive algorithm for the ALIP to diagnose malaria *in vitro*. High sensitivity and specificity was desired, in additional to the inclusion of auxiliary functions that offer novel information to clinicians and researchers.

4.1 Sensitivity and Specificity

The overall sensitivity and specificity of the ALIP was 100% and 97.7%, respectively. The PPV and NPV were 93.8% and 100%, respectively. These values are in reference to the calculated parasitemia as a discrimination threshold. A cutoff of 0.025% was decided upon because it provided the optimal balance of sensitivity, specificity, and lower limit of detection. These values exceed the performance characteristics of the primary field-use diagnostic methods (i.e., microscopy, QBC, and RDT) as reported by various clinical trials and investigations. The accuracy of the image analysis algorithm, as it currently stands, will facilitate early diagnosis of malaria and subsequently contribute to reduced disease transmission in endemic regions. Improved algorithm calculations, as well as the inclusion of new fluorescent fluorophores, could further decrease the false positive rate and subsequently improve the accuracy and lower limit of detection.

4.2 Automatic Calculation of Parasitemia Magnitude

The ability of the system to calculate the magnitude of parasitemia is of critical importance to the clinician because malaria complicacy and severity can be inferred from this parameter (Moody, 2002). There is currently no diagnostic available method capable of automatically calculating the parasitemia of a sample. Performing image analysis techniques on a cell-by-cell basis provides a means for this system to calculate parasitemia magnitude. The described image analysis algorithm is able to perform this task at a much faster rate than a trained microscopist, thereby improving the throughput of clinical laboratories. The current time computation for 100,000 cells is approximately 100 seconds. Assuming an 83% improvement in processing time by conversion from

MATLAB to C++, this could be reduced to 17 seconds or less. For comparison, it takes approximately 60 minutes or more to analyze just 10,000 cells by traditional microscopy methods. Additionally, automation removes the counting error and fatigue of human bias, enabling a more accurate parasitemia calculation to be obtained.

4.3 Sequential CBC and Malaria Diagnosis

A major advantage of the ALIP is the ability to simultaneously obtain a CBC (Wardlaw, 2010a) and diagnose malaria (Levine et al., 2012a; Levine et al. 2012b). Current practice recommends that when a suspect patient is diagnosed for a parasitic disease, a CBC should be performed if a hematology analyzer is readily available (Castelli et al., 1997). Anemia and thrombocytopenia are common in malarial infection and especially so with the *falciparum* species (Giles, 2002; Patel et al., 2004). Hemoglobin (HGB) and platelet count (PLT) are therefore important parameters of the CBC that can improve sensitivity and specificity when used in conjunction with a malarial diagnostic method (Patel et al., 2004). The ability to simultaneously determine HGB and PLT will provide confirmatory information to the clinician and will only improve the sensitivity and specificity of detection by the ALIP.

4.4 Stage Identification

The ability to identify all four stages of erythrocytic malaria infection (i.e., ring, trophozoite, schizont, and gametocyte) can provide clinicians with important information regarding the complicacy of a particular infection. Trophozoites and schizonts are particularly dangerous when in circulation because they are large and abnormally shaped, and can act as an embolus to reduce blood flow to the brain or heart, resulting in a sudden stroke or heart attack. The amount and distribution of gametocytes, the sexual form of malaria, can also provide information regarding the infectivity of a particular patient.

The ALIP is capable of detecting stages based on the presence and amount of hemozoin. The collection of additional human malaria specimen with more advanced stages present in the peripheral blood will allow an algorithm to be developed that categorizes

each intraerythrocytic parasite into a particular stage, ultimately being able to report the exact stage distribution of parasites.

4.5 Blood Transfusion Screening

The system may also find additional utility for blood banks, as there is no approved screening test for blood donors (Mann, 2011). Asymptomatic patients with malaria or babesiosis have the potential to donate blood without knowledge of their infection, which presents potentially serious complications to the recipient. Transfusion-transmitted babesiosis is often severe because the recipient is generally immunocompromised; approximately 20% of such cases result in fatalities (Vannier et al., 2012). Similarly, transmittance of malaria via blood transfusion to a non-immune patient can be rapidly fatal (Owusu-Ofori et al., 2010). Although transfusion transmission of malaria is still relatively rare, these cases are becoming more frequent due to increased worldwide travel in combination with an increased demand for blood transfusion (Saeed et al., 2002). Blood from donors in the sub-Saharan region of Africa is not tested for malaria (Tagny et al., 2008) despite recommendations from the World Health Organization that all donated blood should be tested for malaria where "appropriate and possible" (World Health Organization, 2012). If performed before a transfusion occurs, the diagnosis of malaria using the ALIP will prevent infected blood from being transmitted to accepting patients. Screening for parasitic diseases with this system before symptomatic development will improve the clinical outcome for the patient when treated and contribute to improved vector control by reducing the risk of disease transmission by transfusions.

4.6 Infected Red Blood Cell Indices Calculations

Since every infected RBC can be identified during the cell-by-cell analysis, RBC indices can be computed for all infected RBCs. The mean cell hemoglobin (MCH), mean cell hemoglobin concentration (MCHC) and mean cell volume (MCV) are three parameters that can provide feedback for drug efficacy evaluation and the monitoring of patient status during treatment. This will allow researchers to inoculate malaria cell culture or

initiate a drug treatment in a human patient and then evaluate the MCH, MCHC, and MCV over time. For example, if a drug is designed to kill intraerythrocytic parasites and limit parasitization of hemoglobin, MCH would reflect its ability to do so. This information can help researchers evaluate the effectiveness of new drug candidates in clearing the parasite and limiting the parasite's ability to consume hemoglobin.

4.7 Transmission of Diagnostic Information

If either a wireless or hard-wired internet connection is available, images generated by the ALIP may be instantly transmitted to any physician in the world. Other patient information such as relevant diagnostic parameters, demographics, symptoms, drug treatment, and follow up notes may be documented and stored locally or with the patient's electronic medical record. This feature, along with the ability to easily store data locally, will improve documentation of patient information and reduce clerical errors.

4.8 Result Rapidity and Decreased Turnaround Time

The rapidity of this system is a considerable advantage, as it can produce results in less time than any commercially-available instrument. A malaria diagnosis can be obtained at the point-of-care in potentially less than 10 minutes compared to up to 60 minutes for Giemsa smear review, 20 minutes for RDT, 30 minutes for QBC, and 24 hours for PCR. Thus, the time-to-result of the ALIP is reduced by 83% compared to the gold standard microscopy review (i.e., 60 minutes reduced to 10 minutes). The rapid turnaround time of the ALIP helps to offset the relatively high initial equipment cost because more patients can be screened for malaria with less operator intervention.

4.9 Future Research

4.9.1 Integration of Hemozoin Polarization Detection Method

Healthy human blood typically does not contain anisotropic crystals while in solution. Examples of abnormal anisotropic substances that are rarely, but can potentially be found

in non-dried whole blood, include phagocytized uric acid crystals (seen in acute gout), phagocytized cholesterol crystals (seen in phagocytized intra-arterial plaque), phagocytized Charcot-Leyden crystals (found in degenerating eosinophils), and hemozoin. The examination of blood specimen or other bodily fluid for the presence of anisotropic crystals requires dark field or polarizing microscopy, both of which are expensive and not suitable for field use.

A method for detection of anisotropic crystals, such as hemozoin, is described by Levine et al. in United States Patent No. 2012/0021456 (Levine et al., 2012b). This method can be integrated into the prototype system with minimal cost and hardware adaptations. It may be useful for future research to briefly discuss its practical ability to enhance the diagnostic capability of this system.

In the apparatus and method described by Levine et al. (2012b), light emanating from the light source passes through a polarizing filter and becomes polarized (FIG. 4.1). This polarized light subsequently passes through an isotropic sample chamber to the analyzing filter.

The analyzing and polarizing filters are capable of selective rotation such that they may automatically be aligned in a cross-polarized (i.e., 90° orthogonal disposition) or open orientation. When in an open orientation, all light is capable of passing through the analyzing filter to the optics and detection apparatus. Conversely, when in a cross-polarized configuration, polarized light emanating from the polarizing filter does not pass through the analyzing filter; however, due to the anisotropic nature of hemozoin, light that comes in contact with the hemozoin crystal is altered and allowed to pass through the analyzing filter, manifesting as a single point of light (FIG. 4.2).

The most noteworthy advantage offered by the integration of a polarized method of hemozoin detection is the potential to significantly improve specificity by searching for points of light on a low noise, low interference background. This could be added to the decision criteria and easily implemented into future diagnostic algorithms. This method may also have utility in improved stage identification of malaria parasites and differentiation of malaria from *Babesia* specimen, since *Babesia* is not hematophagous

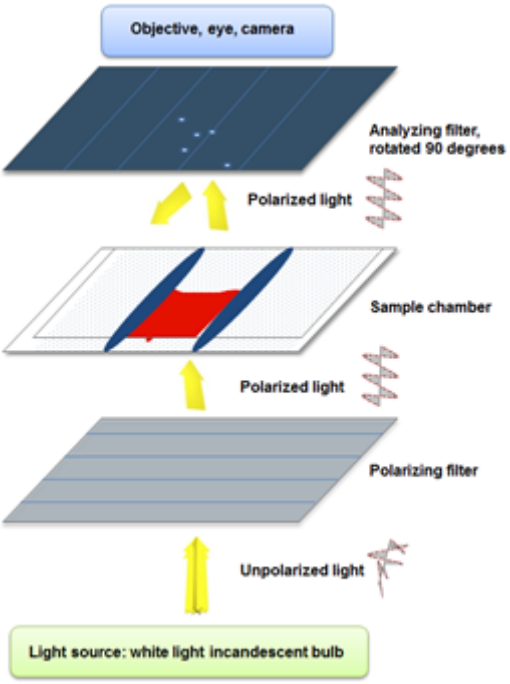

Figure 4.1: Sample chamber disposed between selectively rotating polarizing and analyzing filters in a cross-polarized configuration (Levine et al., 2012b). In this orientation, unpolarized light will become polarized by the polarizing filter and subsequently pass through the sample chamber. Light that interacts with anisotropic malarial hemozoin crystals will be modified and manifest as points of light to the optical detection system.

Figure 4.2: Light emanating from hemozoin crystals in a *P. falciparum* (lifecycle asynchronous) infected 2% HCT RBC culture using a cross-polarized configuration (Levine et al., 2012b). Image captured with a 10X objective lens (0.25 NA) using a 540 nm filter over white light and a 1 second exposure time.

and does not produce hemozoin.

4.9.2 Translation to Other Imaging Modalities

Although the algorithm developed during the course of this research was specifically designed to be used within the ALIP, it is possible to apply similar image processing methods on other available malaria diagnostic methods. A fluorescent microscopy technique, such as the QBC Malaria test, must be used but the fluorophore is not necessarily limited to acridine orange. DAPI or BCP could be alternatively be used, for example. A major limitation of translation to other modalities is that the artifact and noise level of the fluorescent images must be very low. This is possible within the ALIP due to the structure of the chamber, the formation of a monolayer of blood cells, and the distribution of various cells throughout the chamber.

4.9.3 Algorithm Improvements

Any alterations to the algorithm to reduce the false positive rate will enable the lower limit of detection to be decreased and subsequently improve the functionality of the ALIP at low parasitemia levels. Increasing the sensitivity and specificity of the sample will enable malaria to be diagnosed more accurately at earlier stages of infection, ultimately contributing to aversion of more malaria-related deaths and unnecessary antimalarial treatments.

Additionally, the flexibility of the ALIP's software will allow for other clinically-useful functions to be added. For example, the ability to falsely color images to simulate Wright or Giemsa stain could be incorporated into successive iterations to improve parasitic visualization.

4.9.4 Outline for Future Clinical Trials

Equipment availability, insufficient funding, and timing issues unfortunately prevented the conduction of a clinical trial on human subjects. It is important that in future research, a clinical study is performed to comprehensively evaluate the diagnostic perfor-

mance of the prototype system in comparison to current methods. The following outline was developed for an actual clinical trial and will be described in detail to be used as a model for future studies.

Parasitemia, sensitivity, specificity, PPV, NPV, false positive rate (FPR), and false negative rate (FNR) in particular will be compared to the gold standard Giemsa thin film (GTF), RDTs, QBC Malaria Test, PCR, and other available instrumentation (e.g., flow cytometry, etc.). Changes to parasitemia should be measured by each instrument after an appropriate drug treatment protocol (advised by a physician) is distributed.

4.9.4.1 Study Design

The proposed study is a pretest-posttest correlational single-center study located in a malaria endemic region, such as sub-Saharan Africa, due to the availability of infected specimen. Experimental subjects (i.e., those infected with malaria) will be compared to a group of control subjects (i.e., those not infected with malaria) for each diagnostics instrument to evaluate each instruments diagnostic performance (defined as the sensitivity, specificity, PPV, NPV, and parasitemia determination) and ability to determine drug efficacy (defined as the reduction in parasitemia level). Subjects will be requested to return for testing a total of four times following initiation of drug therapy to monitor infection after drug treatment.

4.9.4.2 Subject Inclusion and Exclusion Criteria

The target population is the native population, particularly those that are susceptible to malarial infection and have no documented disease resistance. A total of n=100 subjects infected with malaria (i.e., the experimental group) and n=200 subjects not infected with malaria (i.e., the control group) will provide sufficient statistical power for conclusion validity.

Males and females of all ages will be encouraged to participate. Young children and the elderly are particularly desirable, as these age groups are the most susceptible to

severe complications and mortalities. For this same reason, pregnant woman are also encouraged to participate as unborn children can become substantially debilitated by malaria. Drug treatment protocol is considerably complicated in pregnant women, so these subjects will be monitored closely for adverse events.

Experimental subjects must exhibit a confirmed malarial infection by GTF and cannot be currently treated with an anti-malarial drug. Control subjects must be confirmed by GTF to have no malarial infection. Ideally all species of *Plasmodium* should be included, with a majority of cases being of the species that is most common in the region. Subjects cannot have sickle cell anemia because this condition has been shown to offer resistance to the malaria parasite. Subjects may also not be frequent users of recreational drugs or alcohol, as the potential interference of these substances is unknown.

Subject attrition is expected during each subject's four-week participation. The benefit of a free, rapid diagnosis and treatment is a sensible justification for returning to the clinic, but subjects will also be compensated with malaria insecticide-treated bed netting, long-sleeved clothing, and DEET spray canisters following completion of the study. This should help to further reduce attrition and help to prevent infection transmission on a local scale.

4.9.4.3 Study Procedures

The ALIP will process blood at the same time as peripheral smears, three RDT models, QBC, and ideally PCR as well as a flow cytometer (e.g., Abbott CELL-DYN 4000). Venous blood samples will be collected from the subjects by a trained phlebotomist and transferred into Vacutainer brand blood collection tubes coated with K_2EDTA to prevent platelet aggregation. Tests will immediately be performed on each diagnostics instrument in duplicate. To prevent sampling error, blood will be tested from only one Vacutainer tube and will not be divided into aliquots.

To perform tests on the ALIP, blood thoroughly mixed by inversion ten to twelve times will be collected into a disposable consumable and promptly inserted into the instrument to run the diagnostic sequence. A transfer pipette or disposable septa-puncturing de-

vice would be sufficient to transfer the blood to the consumable bowl. Due to current computation time, data will be stored and processed at a later date.

Peripheral smears will be stained with 10% Giemsa and viewed by a trained technician using a light microscope. Parasitemia levels will be calculated according to the CDC's DPDx standards as discussed in Section 2.2.2.4 and Equation 5 (Centers for Disease Control and Prevention, 2010a). Samples will be considered negative when no parasite is detected in a total of 40 observed fields. The species and stages present in the sample will also be identified.

To perform tests on the QBC malaria system, blood will be collected from a finger stick into the plastic QBC tube by a clinician. The clinician will invert the tube to ensure that the sample is thoroughly mixed with the internally-coated acridine orange and potassium oxalate reagents. A plastic float will be inserted into the capillary tube and the sample will be centrifuged for at least five minutes. An operator with experience using the QBC system will then examine the sample using a conventional light microscope equipped with an ultraviolet adapter and an epi-illuminated microscope objective. A numerical scale described by the manufacturers specifications and performed by Adeoye and Nga (2007) will establish the guideline for parasitemia determination.

Three RDTs will be evaluated, including the Malaria Antigen Pf/Pan, Malaria Ag-Pf, and Ag-Pv (Standard Diagnostics, Seoul, Republic of Korea). Chaijaroenkul et al. (2011) compared these three models to Giemsa-stained peripheral smears and PCR, with good results from each model. Samples will be withdrawn from the Vacutainer and processed on the RDTs according to the manufacturer's specifications. As indicated by each product's user manual, the presence of both the control and test lines will indicate a positive result for *P. falciparum* or *vivax*, whereas the presence of only the control line will indicate a negative result.

If PCR equipment and technicians are readily available, PCR diagnostics will be processed according to the manufacturer's instructions and the methodology described by Fontecha et al. (2012). This will be performed by a laboratory technician familiar with PCR and good laboratory practice (GLP). Nested or un-nested multiplex and single-tube

species-specific PCR will be used depending on the malaria species present. Primer ID and 5'-3' primer sequence will be used to detect *P. falciparum* or *P. vivax*.

If a CELL-DYN 4000 flow cytometer is available, blood will be processed by a technician in accordance with the methods proposed by Wever et al. (2002), otherwise the manufacturing specifications for another flow cytometer will be followed. The Abbott CELL-DYN 4000 was selected because it has reported sensitivity up to 91% and specificity up to 100% (Wever et al., 2002); however, other flow-cytometer or impedance analyzers can be used depending on their availability at the clinical site.

If a subject tests positive for malaria, they will be instructed to consult with an attending physician on treatment options. Subjects will have the option to return for additional testing or opt out of the study, regardless of their drug treatment protocol. Control subjects will be given a placebo drug and instructed to ingest at identical intervals as the infected group. It is considered unethical to deny malaria-positive patients

Subjects will return at days one, two, three, and five after treatment with anti-malaria drugs. All diagnostics tests will be performed during each visit using the same protocol discussed above. Changes to each subject's symptoms, complete blood count (as determined by the prototype system and flow cytometer for reference) and RBC morphological changes (as determined by Giemsa peripheral smears) will be noted. Vital signs such as body temperature, blood pressure, blood oxygen saturation, and cardiac rhythmicity will be monitored to ensure patient safety during the trial.

4.9.4.4 Data Analysis and Interpretation

The sensitivity, specificity, PPV, NPV, FPR, FNR, and parasitemia level will be recorded for all reference instruments and compared to the prototype. Linear interpolation of parasitemia level will be performed so that the coefficient of determination (R^2) may be calculated.

To evaluate drug efficacy, all parameters will again be computed after the subject has been treated for malaria. Drug efficacy has been defined as the reduction in parasitemia level. Therefore, the percent difference in parasitemia from before drug treatment to after

drug treatment (at days one, two, three, and five) will be recorded for all instruments. The ability for each instrument to detect morphological changes of both RBCs and parasites will also be noted. If the instrument is capable of doing so, the quality of morphology detection, in terms of resolution and contrast, will be a comparable parameter. Only the imaging prototype, QBC, and GTF are capable of detecting cell morphology.

An ROC curve will be generated to evaluate the sensitivity and false positive rate of the prototype using various parasitemia threshold levels. This analysis can be used to improve the performance of the ALIP for future research and ultimately, clinical practice.

4.9.4.5 Clinical Trial Implementation

The method described herein is meant to be used as a model for future clinical trials using the prototype instrument. It may need to be altered depending on resource availability and other factors. As described, this outline should provide sufficient validity and statistical power to evaluate the diagnostic performance and overall potential of the ALIP.

5 Conclusion

The image analysis methodology described in this thesis is capable of having a uniquely positive clinical impact around the world by providing a rapid malarial screening method that enables critical information to be automatically determined without the need for review by a trained technician.

The overall goal of this research was to develop an image analysis algorithm with at least 95% sensitivity and 95% specificity with the initial application using the Abbott Laboratories Imaging Platform (ALIP). The image analysis algorithm exhibited a sensitivity of 100% (n=1 positive malaria human subject) and a specificity of 97.7% (n=22 negative malaria human subjects). Although the sample size of this study was small, the accuracy of this system and image processing methodology was actually superior to the primary field-use malaria diagnostic instruments. Additional clinical testing should be performed to comprehensively evaluate the diagnostic performance of the ALIP with an increased statistical power; however, the detection ability of the current image analysis algorithm offers some distinct advantages for the early diagnosis of malaria and the consequential prevention of disease transmission.

The primary objective of this research was to fully utilize the flexibility of the existing imaging technology to integrate auxiliary features to generate clinically-useful information that is not currently available with automated methods.

The image analysis algorithm was configured to automatically calculate parasitemia magnitude and was able to accurately compute this parameter with an 83% reduction in time compared to the gold standard microscopy review. This will allow clinicians to determine the severity of a particular infection more rapidly and be able to treat the patient earlier.

Hemoglobin and platelet parameters were simultaneously reported with the malaria diagnosis in addition to other parameters of the CBC. Low hemoglobin and platelet concentrations are indicative of malaria infection and can be used in conjunction with the ALIP diagnosis to confirm or reject reported results. This will help to improve the sensitivity and specificity of detection.

All four erythrocytic stages from cell culture specimen were identifiable by the ALIP. The collection of additional human specimen with more advanced stages will permit the development of an automated algorithm to calculate the parasitic stage distribution. This will give clinicians a perspective of the disease severity and the probability that the larger stages (i.e., trophozoite and schizont) may act as emboli and disrupt blood flow to the brain or heart.

Infected RBC indices (i.e., MCH, MCHC, and MCV) were calculated from a plurality of 145 ring-stage infected RBCs. The data demonstrated minimal variation in the MCH and MCHC compared to uninfected RBCs, but an increase of 2.8 fL in the cell volume of infected RBCs. This data indicates that hemoglobin was not substantially consumed by the parasite, and that the infected RBC volume increased due to the inclusion of the parasite. The ability to calculated infected RBC indices will provide useful information for researchers in the development of new drug candidates, as well as monitoring a patient's reaction to a particular anti-malarial treatment.

Diagnostic information (i.e., infected cell images, parasitemia measurements, etc.) was successfully transmitted using a SMTP. This will allow clinicians anywhere in the world to be able to interpret images to confirm or reject diagnostic results. The ability to save and recall images locally will also allow clinicians to interpret results at the point of care for a more rapid confirmation.

The time-to-result using the current MATLAB image analysis algorithm was approximately 60 minutes but, when the algorithm is ultimately converted to C++, the time from sample acquisition to result can potentially be reduced to less than 10 minutes. This time requirement is less than each of the primary field-used diagnostic instruments, allowing more patients to be screened with minimal operator intervention. The application of the algorithm using the ALIP demonstrates that much more information is possible and in less time than any currently available technology.

In summary, the objectives of this research were accomplished and the result is the production of an exceptionally useful diagnostics instrument. The information made available to clinicians will allow them to make a more informed diagnosis and determine

appropriate treatment methods on a patient-by-patient basis. This instrument will also contribute in the early detection of malaria, thereby reducing the mortality rate due to infectious transfusions, limit unnecessary exposure to antimalarial drugs, and improve resource waste in endemic regions. The application of the image processing methodology described in this thesis has the potential to have a significant impact on global health and, with further research and development, this system could be introduced to the regions of the world that need it most, so that its true potential may be realized.

6 References

Abbott Hematology (2010a). CELL-DYN Emerald Operator's Manual. List Number 09H40-01.

Abbott Hematology (2010b). "Abbott Hematology, CELL-DYN Emerald." *CAP Today.* http://www.captodayonline.com/productguides/instruments/hematology-analyzers/abbott-hematology-cell-dyn-emerald.html.

Adeoye, G. O., Nga, I. C. (2007). Comparison of Quantitative Buffy Coat technique (QBC) with Giemsa-stained thick film (GTF) for diagnosis of malaria. *Parasitology International.* **56**: 308-312.

Bill and Melinda Gates Foundation. (2011). Malaria Strategy Overview. http://www.gatesfoundation.org/malaria/Documents/malaria-strategy.pdf.

Castelli, F., and G. Carosi. (1997). "Diagnosis of malaria infection." *Handbook of Malaria Infection in the Tropics.* http://www.aifo.it/english/resources/online/books/other/malaria/contents.htm.

Centers for Disease Control and Prevention. (2005a). Public Health Image Library (PHIL). Identification #7861. http://phil.cdc.gov/phil/home.asp.

Centers for Disease Control and Prevention. (2005b). Public Health Image Library (PHIL). Identification #7315. http://phil.cdc.gov/phil/home.asp.

Centers for Disease Control and Prevention. (2010a). "Laboratory diagnosis of malaria." Laboratory Identification of Parasites of Public Health Concern. http://dpd.cdc.gov/dpdx/HTML/Malaria.htm

Centers for Disease Control and Prevention. (2010b) "Malaria Treatment (United States)." Centers for Disease Control. http://www.cdc.gov/malaria/diagnosis_treatment/treatment.html.

Centers for Disease Control and Prevention (2010c). Diagnostic Findings: Malaria. *CDC Center for Global Health.*

http://www.dpd.cdc.gov/DPDX/HTML/Frames/MR/Malaria/falciparum/body_malariadffalcschi.htm

Centers for Disease Control and Prevention. (2011a). "Guidelines for Treatment of Malaria in the United States." *Centers for Disease Control.* http://www.cdc.gov/malaria/resources/pdf/treatmenttable.pdf.

Centers for Disease Control and Prevention. (2011b). "Treatment of Malaria (Guidelines For Clinicians)." *Centers for Disease Control.* http://www.cdc.gov/malaria/resources/pdf/clinicalguidance.pdf.

Chaijaroenkul, W., Wongchai, T., Ruangweerayut, R., Na-Bangchang, K. (2011). Evaluation of Rapid Diagnostics for Plasmodium falciparum and P. vivax in Mae Sot Malaria Endemic Area, Thailand. *Korean Journal of Parasitology.* **49**(1): 33-38.

Coulter, W. H. (1956). High Speed Automatic Blood Cell Counter and Cell Size Analyzer. *Proceedings of the National Electronics Conference.* **12**: 1034-1040.

DeNicola, D. (2011). Advances in Hematology Analyzers. *IDEXX Laboratories.* 52-61.

Estacio, R. H., Dy, E. E. R., Cresswell, S., Coronel, R. F., Alora, A. T. (1993). The Quantitative Buffy Coat Technique (QBC) in Early Diagnosis of Malaria: The Santo Tomas University Hospital Experience. *Philippine Journal of Microbiology and Infectious Disease.* **22**(2).

Fawcett, T. (2006). An Introduction to ROC Analysis. *Pattern Recognition Letters.* **27**: 861-874.

Fontecha, G. A., Mendoza, M., Banegas, E., Poorak, M., De Oliveira, A. M., Mancero, T., Udhayakumar, V., Lucchi, N. W., Mejia, R. E. (2012). Comparison of molecular tests for the diagnosis of malaria in Honduras. *Malaria Journal.* **11**: 119.

Frischknecht, F., Baldacci, P., Martin, B., Zimmer, C., Thiberge, S., Olivo-Marin, J., Shorte, S. L., Mnard. (2004). Imaging movement of malaria parasites during transmission by Anopheles mosquitoes. *Cellular Microbiology.* **6**(7): 687-694.

Giles, H. M. (2002). Handbook of Malaria Infection in the Tropics. *International Health Cooperation.* Chapter 6: Pathology of Malaria.

Girosi, F., Olmsted, S. S., Keeler, E., Burgess, D. C. H., Lim, Y., Aledort, J. E., Rafael, M. E., Ricci, K. A., Boer, R., Hilborne, L., Derose, K. P., Shea, M. V., Beighley, C. M., Dahl, C. A., Wasserman, J. (2006). Developing and interpreting models to improve diagnostics in developing countries. *Nature.* **444**(1): 3-8.

Goldsmith, B. (2004). Optimizing Point-of-care testing. *Merion Matters.* http://laboratory-manager.advanceweb.com/editorial/content/editorial.aspx?cc=38611.

Greenberg, A. E., Ntumbanzondo, M., Ntula, N., Mawa, L., Howell, J., Davachi, F. (1989). Hospital-based surveillance of malaria-related paediatric morbidity and mortality in Kinshasa, Zaire. *Bulletin of the World Health Organization.* **67**(2): 189-96.

Guyton, A., Hall, J. (2011). *Textbook of Medical Physiology.* 12th ed. Philadelphia, PA: Elsevier. Print.

Hawkes, M., Kain, K. C. (2007). Advances in malaria diagnosis. *Expert Review of Anti-infective Therapy.* **3**: 485-495.

Hempelmann, E. (2008). *P. falciparum* schizont. http://en.wikipedia.org/wiki/File:P.falciparum_schizont.jpg.

Holmes, D., Pettigrew, D., Reccius, C. H., Gwyer, J.D., van Berkel, C., Holloway, J., Davies, D. E., Morgan, H. (2009). Leukocyte analysis and differentiation using high speed microfluidic single cell impedance cytometry. *Royal Society of Chemistry.* **9**: 2881-2889.

Horecker, B. L. (1942). The Absorption Spectra of Hemoglobin and its Derivatives in the Visible and Near Infra-red Regions. *The Division of Industrial Hygiene, National Institute of Health*, 173-183.

Hudson, K. (2005). Get bedside results with point of care testing. *Nursing Management*. **36**: 45-46.

Invitrogen. (2012). Acridine Orange. http://products.invitrogen.com/ivgn/product/A1301.

Izumo, A., Tanabe, K., Kato, M. (1987). A method for monitoring the viability of malaria parasites (*Plasmodium yoelii*) freed from the host erythrocytes. *Transactions of the Royal Society of Tropical Medicine and Hygiene*. **81**: 264-267.

Jones, C.S., Mayfield, S.P. (2012). Steps toward a globally available malaria vaccine: Harnessing the potential of algae for future low cost vaccines. *Bioengineered*. **4**(3).

Kawamoto, F., Billingsley, P. F. (1992). Rapid Diagnosis of Malaria by Fluorescence Microscopy. *Lancet*. **337**: 200-202.

Keiser, J., Utzinger, J., Premji, Z., Yamagata, Y., Singer, B. H. (2002). Acridine Orange for malaria diagnosis: its diagnostics performance, its promotion and implementation in Tanzania, and the implications for malaria control. *Annals of Tropical Medicine & Parasitology*. **97**: 643-654.

Lee-Lewandrowski, E., Gregory, K., Lewandrowski, K. (2010). Point of care testing in a large urban academic medical center: evolving test menu and clinical applications. *Clinical Chimica Acta*. **411**: 1799-1805.

Lee-Lewandrowski, E., Lewandrowski, K. (2009). Perspectives on Cost and Outcomes for Point-of-Care Testing. *Clinics in Laboratory Medicine*. **29**: 479-489.

Levine, R. A., Wardlaw, S. C., Patton, C. L. (1989). Detection of hematoparasites using quantitative buffy coat analysis tubes. *Parasitology Today*. **5**(4): 132-134.

Levine, R., Jorgensen, M. (2012a). "A Method and Apparatus for Detecting the Presence of Intraerythrocytic Parasites". US Patent Application 13/630,934. 28 Sep 2012.

Levine, R. A., Unfricht, D. W., Wardlaw, S. C., Ports, B. (2012b). "Method and Apparatus for Detecting the Presence of Anisotropic Crystals and Hemozoin Producing Parasites in Liquid Blood". U.S. Patent Publication 2012/0021456. 26 Jan 2012.

Lewandrowski, K. (2009). Point-of-Care Testing: An Overview and a Look to the Future. *Clinics in Laboratory Medicine*. **29**: 421-432.

Lewandrowski, K., Gregory, K., Macmillan, D. (2011). Assuring Quality in Point-of-Care Testing. *Archives of Pathology & Laboratory Medicine* **135**: 1405-1414.

Life Technologies Corporation. (2012). Product Spectra - Acridine orange/DNA. http://tinyurl.com/aoulpxv.

Life Technologies Corporation. (2013). Molecular Probes fluorescent organelle stains - Table 12.1. http://www.invitrogen.com/site/us/en/home/References/Molecular-Probes-The-Handbook/tables/Molecular-Probes-organelle-selective-probes.html.

Makler, M.T., Ries, L. K., Ries, J., Horton, R. J., Hinrichs, D. J. (1991). Detection of Plasmodium Falciparum Infection with the Fluorescent Dye, Benzothiocarboxypurine. *The American Journal of Tropical Medicine and Hygiene*. **44**(1): 11-16.

Mann, Denise. (2011). "Tick-borne Illness May Lurk in Blood Supply: Researchers say screening test for babesiosis in donated blood needed." *US News & World Report*. http://health.usnews.com/health-news/managing-your-healthcare/articles/2011/09/05/tick-borne-illness-may-lurk-in-blood-supply.

Mathers C. D., Loncar D. (2006). Projections of Global Mortality and Burden of Disease from 2002 to 2030. *PLoS Med*. **3**(11): e442.doi:10.1371/journal.pmed.0030442.

Maxmen, Amy. (2012a). Malaria plan under scrutiny. *Nature*. **490**. 13-14.

Maxmen, Amy. (2012b). Malaria surge feared. *Nature*. **485**: 293.

Melhorn, H., Schein, E. (1984). The piroplasms: life cycle and sexual stages. *Advances in Parasitology*. **23**: 37-103.

Meyer, F. (1994). "Topographic distance and watershed lines". *Signal Processing.* **38**: 113-125.

Michalakis, Y., Renaud, F. (2009). Evolution in vector control. *Nature.* **462**(19): 298-300.

Moody, A. (2002). Rapid Diagnostic Tests for Malaria Parasites. *Clinical Microbiology Reviews.* **15**(1): 66-78.

National Geographic Society. (2012). Photo Gallery: Malaria. Malaria Parasites Amid Red Blood Cells. http://tinyurl.com/b63tm42.

National Institute of Allergy and Infectious Diseases. (2012). Life Cycle of the Malaria Parasite. *National Institutes of Health.* Web. 13 Oct 2012. http://www.niaid.nih.gov/topics/malaria/pages/lifecycle.aspx

Nkrumah, B., Agyekum, A., Acquah, S. E. K., May, J., Tannich, E., Brattig, N., Nguah, S. B., von Thien, H., Adu-Sarkodie, Y., Huenger, F. (2010). Comparison of the Novel Partec Rapid Malaria Test to the Conventional Giemsa Stain and the Gold Standard Real-Time PCR. *Journal of Clinical Microbiology.* **48**(8): 2925-2928.

Ogunbajo, A. (2011). Migration of Plasmodium Sporozoites through Host Cells. *Journal of the Student National Medical Association.*

Owusu-Ofori, A. K., Parry, C., Bates, I. (2010). Transfusion-Transmitted Malaria in Countries Where Malaria Is Endemic: A Review of the Literature from Sub-Saharan Africa. *Clinical Infectious Diseases.* **51**(10): 1192-1198.

Ozcan, Aydogan. (2010). "Telemedicine Microscopy toward Smart Global Health Systems." *University of California, Los Angeles.* http://launch.org/presentations/LUCAS.pdf.

Partec. (2012). Partec Essential Healthcare: Malaria. http://www.partec.com/applications/essential-healthcare/malaria.html.

Patel, U., Gandhi, G., Friedman, S., Niranjan, S. (2004). Thrombocytopenia in Malaria. *Journal of the National Medical Association*. **96**(9): 1212-1214.

Payne, D. (1988). Use and limitations of light microscopy for diagnosing malaria at the primary health care level. *Bulletin of the World Health Organization*. **66**(5): 621-626.

PixCell Medical. (2010). "Overview-Products and Applications." PixCell Ltd. http://www.pixcell-medical.com/products.asp.

Prahl, S. (1999). Optical Absorption of Hemoglobin. http://omlc.ogi.edu/spectra/hemoglobin/index.html.

QBC Diagnostics. (2012). QBC Malaria Test: Frequently Asked Questions (FAQs). *QBC Diagnostics*. Web. 08 Nov 2012. http://www.qbcdiagnostics.com/products/fm/malaria/faq.asp#f10

Rafael, M. E., Taylor, T., Magill, A., Lim, Y., Girosi, F., Allan, R. (2006). Reducing the burden of childhood malaria in Africa: the role of improved diagnostics. *Nature*. **444**(1): 39-48.

Reyburn, H., Mbatia, R., Drakeley, C., Carneiro, I., Mwakasungula, E., Mwerinde, O., Saganda, K., Shao, J., Kitua, A., Olomi, R., Greenwood, B. M., Whitty, C. J. M. (2004). Overdiagnosis of malaria in patients with severe febrile illness in Tanzania: a prospective study. *British Medical Journal*. **329**(7476).

RnCeus.com. (2006). White Blood Cell Count (WBC) and Differential. http://www.rnceus.com/cbc/cbcwbc.html.

Saeed, A. A., Mohsen Al Rasheed, A., Al Nasser, I., Al Onaizi, M., Al Kahtani, S., Dubois, L. (2002). Malaria Screening of Blood Donors in Saudi Arabia. *Annals of Saudi Medicine*. **22**(5-6): 329-332.

Sanofi Aventis. (2002). Artifacts commonly mistaken for malaria parasites. (2002). http://www.impact-malaria.com/web/malaria_training/identification_species/artefacts

ScienceDaily. (2007). Science News. Cerebral Malaria: Approaching A Diagnostic Test. http://www.sciencedaily.com/releases/2007/05/070503100808.htm

Sears, D. A., Udden, M. M. (2012). Howell-Jolly Bodies: A Brief Historical Review. *The American Journal of the Medical Sciences*. **343**(5): 407-409.

Srinivasan, S., Moody, A. H., Chiodini, P. L. (2000). Comparison of blood-film microscopy, the OptiMAL® dipstick, Rhodamine-123 fluorescence staining and PCR, for monitoring antimalarial treatment. *Annals of Tropical Medicine and Parasitology*. **94**(3): 227-232.

Sun, Y., Moreau, E., Chauvin, A., Malandrin, L. (2011). The invasion process of bovine erythrocyte by *Babesia* divergens: knowledge from an in vitro assay. *Veterinary Research*. **42**: 62.

Tagny, C. T., Mbanya, D., Tapko, J., Lefre're, J. (2008). Blood safety in sub-Saharan Africa: a multi-factorial problem. *Transfusion*. **48**(6): 1256-1261.

Tangpukdee, N., Duangdee, C., Wilairatana, P., Krudsood, S. (2009). Malaria Diagnosis: A Brief Review. *Korean Journal of Parasitology*. **47**(2): 93-102.

Tek, F. B., Dempster, A. G., Kale, I. (2009). Computer Vision for Microscopy Diagnosis of Malaria. *Malaria Journal*. **8**(153).

van den Boomgard, R, R. van Balen. (1992). "Methods for Fast Morphological Image Transforms Using Bitmapped Images". *Computer Vision, Graphics, and Image Processing: Graphical Models and Image Processing*, **54**(3): 254-258.

Vannier, E., Krause, P. J. (2012). Human Babesiosis. *New England Journal of Medicine*. **366**(25): 2397-2407.

Verrant, J. A., Lalpuria, N. V., Nikonorov, I., Unfricht, D. W., Ports, B., Wardlaw, S. C., Levine, R. A., Holt, R., Hukari, K. (2012). "Biologic Fluid Analysis Cartridge with Sample Handling Portion and Analysis Chamber Portion". U.S. Patent Publication 2012/0219457. 30 Aug 2012.

Villarreal, M. R. (2008). *Babesia* life cycle human. http://en.wikipedia.org/wiki/File:Babesia_life_cycle_human_en.svg.

Wadsworth Center. (2012). Through the Microscope: Blood Cells - Life's Cells. http://www.wadsworth.org/chemheme/heme/microscope/pltsatellitosis.htm.

Walsh, Michael. (2011). Infection Landscapes. A consideration of the epidemiology, ecology, and physical and social landscapes of infectious diseases. http://www.infectionlandscapes.org/2011/02/lyme-disease.html.

Wardlaw, S. C. (2002). "Apparatus for Analyzing Biologic Fluids". US Patent 2002/0028158 A1. 07 March 2002.

Wardlaw, S. C. (2005). "Apparatus for Analyzing Biologic Fluid". U.S. Patent 6,869,570. 22 Mar 2005.

Wardlaw, S. C. (2010a). "Apparatus for Performing Counts Within a Biologic Fluid Sample". U.S. Patent Publication 2010/0273244. 28 Oct 2010.

Wardlaw, S. C. (2010b). "Disposable Chamber for Analyzing Biologic Fluids". U.S. Patent Publication 2010/0216248. 26 Aug 2010.

Wardlaw, S. C., Levine, R. A., Unfricht, D. W., Lalpuria, N. V., Hill, J. R. (2011). "Method and Apparatus for Determining Red Blood Cell Indices of a Blood Sample Utilizing the Intrinsic Pigmentation of Hemoglobin Contained Within the Red Blood Cells". U.S. Patent 7,903,241. 8 Mar 2011.

Wardlaw, S. C. (2012). "Disposable Chamber for Analyzing Biologic Fluids". U.S. Patent 8,241,572. 14 Aug 2012.

Wever, P. C., Henskens, Y. M. C., Kager, P. A., Dankert, J., van Gool, T. (2002). Detection of Imported Malaria with the CELL-DYN 4000 Hematology Analyzer. *Journal of Clinical Microbiology.* **40**(12): 4729-4731.

Wikipedia. (2006). Receiver Operating Characteristic. http://en.wikipedia.org/wiki/File:Receiver_Operating_Characteristic.png

Williams, I. (2013). Drug-resistant malaria in Thailand threatens deadly global 'nightmare'. *NBC News*. http://tinyurl.com/aqwug3e.

Wilson, M. L. (2012). Malaria Rapid Diagnostic Tests. *Medical Microbiology*. **54**(11): 1637-1641.

World Health Organization. (2006). Guidelines for the Treatment of Malaria. WHO/HTM/MAL/2006.1108.

World Health Organization. (2009). "Online Q&A." http://www.who.int/features/qa/26/en/index.html.

World Health Organization. (2010). Malaria Fact Sheet No 94. http://www.who.int/mediacentre/factsheets/fs094/en.

World Health Organization. (2012). Blood transfusion safety: testing of donated blood. http://www.who.int/bloodsafety/donation_testing/en/